Article

SOURCE DATA | TRANSPARENT PROCESS | OPEN ACCESS

THE EMBO JOURNAL

A mitochondrial EglN1-AMPKα axis drives breast cancer progression by enhancing metabolic adaptation to hypoxic stress

Weiwei Jiang[1,†], Mengyao Zhang[1,†], Chuan Gao[1,†], Chaojun Yan[1], Ronghui Gao[1], Ziwei He[1], Xin Wei[2], Jingjing Xiong[1], Zilun Ruan[3], Qian Yang[4], Jinpeng Li[4], Qifang Li[1], Ziyi Zhong[1], Mengna Zhang[1], Qianqian Yuan[4], Hankun Hu[5], Shuang Wang[6], Ming-Ming Hu[3], Cheguo Cai[1], Gao-Song Wu[4], Chao Jiang[2], Ya-Lin Zhang[7], Chen-Song Zhang[7] & Jing Zhang[1,8,9,*]

Abstract

Mitochondria play essential roles in cancer cell adaptation to hypoxia, but the underlying mechanisms remain elusive. Through mitochondrial proteomic profiling, we here find that the prolyl hydroxylase EglN1 (PHD2) accumulates on mitochondria under hypoxia. EglN1 substrate-binding region in the β2β3 loop is responsible for its mitochondrial translocation and contributes to breast tumor growth. Furthermore, we identify AMP-activated protein kinase alpha (AMPKα) as an EglN1 substrate on mitochondria. The EglN1-AMPKα interaction is essential for their mutual mitochondrial translocation. After EglN1 prolyl-hydroxylates AMPKα under normoxia, they rapidly dissociate following prolyl-hydroxylation, leading to their immediate release from mitochondria. In contrast, hypoxia results in constant EglN1-AMPKα interaction and their accumulation on mitochondria, leading to the formation of a Ca^{2+}/calmodulin-dependent protein kinase 2 (CaMKK2)-EglN1-AMPKα complex to activate AMPKα phosphorylation, ensuring metabolic homeostasis and breast tumor growth. Our findings identify EglN1 as an oxygen-sensitive metabolic checkpoint signaling hypoxic stress to mitochondria through its β2β3 loop region, suggesting a potential therapeutic target for breast cancer.

Keywords AMPKα; EglN1; hypoxia; metabolic homeostasis; mitochondrial translocation

Subject Categories Cancer; Metabolism

DOI 10.15252/embj.2023113743 | Received 12 February 2023 | Revised 26 July 2023 | Accepted 27 July 2023 | Published online 4 September 2023

The EMBO Journal (2023) 42: e113743

Introduction

Breast cancer is the most common cancer among women and the second leading cause of cancer-related death with the highest cancer incidence rate (Siegel *et al*, 2022). Hypoxia leads to metabolic reprogramming and advanced tumor progression, which is associated with high-grade breast tumor and poor prognosis of breast cancer patients, improved understanding of how cancer cell survives under hypoxia has advanced the development of effective therapies (Nakazawa *et al*, 2016; Bhandari *et al*, 2019; Ye *et al*, 2019). For example, hypoxia-inducible factor (HIF) is a well-established regulator that drives cellular adaptation to hypoxia. Under normoxia, HIFα is hydroxylated by the prolyl hydroxylases EglN1/2/3, and the hydroxyl modification is then targeted by the von Hippel Lindau (VHL) E3 ligase complex for subsequent ubiquitylation and proteasomal degradation (Kaelin & Ratcliffe, 2008). Under hypoxia, HIFα is stabilized due to suppression of prolyl hydroxylation, and dimerizes with HIF1β (ARNT), consequently activating oncogenic processes such as angiogenesis (*e.g.*, via *VEGF*), glycolysis and glucose transport (*e.g.*, via *GLUT1*), and erythropoiesis (*e.g.*, via *EPO*) (Yang & Kaelin, 2001; Semenza, 2012). Emerging evidence support that sophisticated interaction networks beyond the HIF pathway contribute to cellular adaptation to hypoxia (Lee *et al*, 2015, 2020b; Guo *et al*, 2016; Zhang *et al*, 2018; Batie *et al*, 2019; Chakraborty *et al*, 2019; Hu *et al*, 2020; Liu *et al*, 2020, 2022).

Mitochondria, the largest consumers of intracellular oxygen, are first in line to confront the fluctuations in oxygen level and

1 Department of Thyroid and Breast Surgery, Medical Research Institute, Frontier Science Center for Immunology and Metabolism, Zhongnan Hospital of Wuhan University, Wuhan University, Wuhan, China
2 Life Sciences Institute, Zhejiang University, Hangzhou, China
3 Frontier Science Center for Immunology and Metabolism, Wuhan University, Wuhan, China
4 Department of Thyroid and Breast Surgery, Zhongnan Hospital of Wuhan University, Wuhan University, Wuhan, China
5 Department of Pharmacy, Zhongnan Hospital of Wuhan University, School of Pharmaceutical Sciences, Wuhan University, Wuhan, China
6 Mabnus Biological Technology Incorporation, Wuhan, China
7 State Key Laboratory for Cellular Stress Biology, Innovation Center for Cell Signaling Network, School of Life Sciences, Xiamen University, Fujian, China
8 Cancer Precision Diagnosis and Treatment and Translational Medicine Hubei Engineering Research Center, Zhongnan Hospital of Wuhan University, Wuhan, China
9 Wuhan Research Center for Infectious Diseases and Cancer, Chinese Academy of Medical Sciences, Wuhan, China
*Corresponding author. Tel: 86 18062556849; E-mail: jing_zhang@whu.edu.cn
†These authors contributed equally to this work

the primary sites for hypoxia-induced metabolic reprogramming (Lee *et al*, 2020b). It has been reported that mitochondrial adaptation to hypoxia is mediated by HIF-induced transcription of the nuclear-encoded COX4 isoform 2 (COX4I2), the mitochondrial protease LON, lactate dehydrogenase A (LDHA) and pyruvate dehydrogenase kinase (PDK1) to modulate ETC activity and the TCA cycle (Iyer *et al*, 1998; Kim *et al*, 2006; Papandreou *et al*, 2006; Lee *et al*, 2020b). Hypoxia also promotes the generation of superoxide through the mitochondrial electron transport chain (ETC) in a HIF-independent manner (Bell & Chandel, 2007), the superoxide leads to accumulation of excess Ca^{2+}, resulting in Ca^{2+}/calmodulin-dependent protein kinase (CaMKK) activation and subsequently stimulating the energy sensor AMP-activated protein kinase (AMPK) to inhibit anabolism (e.g., lipid synthesis) and promote catabolism (e.g., autophagy) for restoring metabolic homeostasis (Emerling *et al*, 2009; Gusarova *et al*, 2011; Mungai *et al*, 2011; Garcia & Shaw, 2017). Although mitochondria are well-known as intracellular platforms for protein–protein interactions to initiate cell signaling (Tan & Finkel, 2020; Picard & Shirihai, 2022), how they serve as scaffolds for oxygen sensing signaling and therefore communicate their fitness to the rest of the cell under hypoxic stress is not well understood. In this study, we demonstrate the prolyl hydroxylase EglN1 as responsible for mitochondrial hypoxia sensing through its β2β3 loop region to control metabolic homeostasis and breast cancer progression.

Results

EglN1 accumulates on mitochondria upon hypoxia

In order to investigate how mitochondria respond to hypoxia, we first profiled the mitochondrial proteome under hypoxia versus normoxia in T47D breast cancer cell line using a TMT-based quantitative proteomics approach (Fig 1A). A total of 5,981 proteins were identified in the mitochondrial extracts, with 569 proteins increased and 477 proteins decreased in relative abundance under hypoxia (Figs 1B and EV1A–C). The network analysis showed the proteins that were involved in oxygen-related pathways (Fig EV1D). In particular, the prolyl hydroxylase EglN1 was identified among the significantly upregulated proteins responsive to hypoxia (Figs 1B and EV1D). Moreover, 2-oxoglutarate-dependent dioxygenases (2OGDDs) are known to have the potential to sense oxygen to regulate the functions of their specific substrates (Losman *et al*, 2020). We found a set of 2OGDDs that were localized to mitochondria, EglN1 is the top-ranked family member in the upregulated group upon hypoxia (Fig 1B). EglN1 is an oxygen sensor involved in the canonical oxygen sensing pathway EglN-VHL-HIF (Kaelin & Ratcliffe, 2008), but its localization and function on mitochondria have not been documented. Subcellular fractionation confirmed that EglN1 was upregulated on mitochondria under hypoxia in different cell lines including T47D, MDA-MB-231, and 293T cell lines (Fig 1C and D). Proteinase K digestion showed that EglN1 was localized on the mitochondrial outer membrane (Fig 1E).

Figure 1. EglN1 accumulates on mitochondria under hypoxia.

A Schematic representation of strategy for identification of mitochondrial proteins by mass spectrometry.
B Rank order of protein signals in mitochondrial proteome of T47D cells exposed to hypoxia (1% O_2 for 24 h) versus normoxia. 2-oxoglutarate-dependent dioxygenases were highlighted. Red, upregulated; blue, downregulated; gray, not significant.
C Immunoblots of extracts from whole cell (WCE), mitochondria (Mito), and cytosol (Cyto) of T47D cells treated with hypoxia (H, 1% O_2 for 24 h) or normoxia (N).
D Immunoblots of extracts from whole cell (WCE), mitochondria (Mito), and cytosol (Cyto) as indicated of MDA-MB-231 and 293T cells treated with hypoxia (H, 1% O_2 for 24 h) or normoxia (N).
E Immunoblots of hypoxic (1% O_2 for 24 h) 293T mitochondrial extract (Mito) treated with indicated concentration of proteinase K for 1 h.
F Immunoblots of extracts from whole cell (WCE) and mitochondria (Mito) of T47D infected with EglN1-Flag followed by treatment with hypoxia (1% O_2 for 24 h) or normoxia.
G Immunofluorescence of T47D cells infected with EglN1-GFP (green) followed by treatment with normoxia or hypoxia (1% O_2 for 24 h) and with MitoTracker Red staining for 15 min. Nuclei were stained with DAPI (blue) (scale bar = 10 μm).
H Quantification of each cells' area overlap ratio for co-localization of EglN1-GFP and mitochondria from (G) (N = 6 images in total).
I Immunoblots of extracts from mitochondria (Mito) as indicated of T47D cells treated with hypoxia (1% O_2) for 0, 12, 24 and 48 h, respectively.
J Immunoblots of extracts from mitochondria (Mito) as indicated of T47D cells treated with normoxia or hypoxia (1% O_2)-reoxygenation (H-ReO_2) for 0, 3, and 6 h, respectively.
K EglN1 expression in breast cancer and normal subtypes in METABRIC cohort (n = 1,139). Wilcoxon rank-sum test was used for statistical analysis of these two groups.
L EglN1 expression in different oxygen levels in METABRIC cohort (n = 1,139). The hypoxia score of METABRIC breast cancer cohort was calculated by using mRNA-based signatures. Kruskal–Wallis test was used for the statistical analysis of these three groups.
M EglN1 expression in different breast cancer subtypes in METABRIC cohort (n = 1,139). METABRIC breast cancer cohort was categorized into five subtypes according to Pam50 gene expression subtype classification (Basal-like, Claudin-low, Her2, Luminal A, and Luminal B). Kruskal–Wallis test was used for the statistical analysis of these multiple groups.
N Representative immunofluorescence of EglN1 and TOM20 with tumor tissues from breast cancer patients. The right panel showed the quantification of fluorescence intensity of TOM20 and EglN1 along the line in merged image.
O Box plot showing the co-localization statistics of EglN1 with TOM20 in these six breast cancer patient samples (n = 6). Y-axis indicates the co-location coefficient of EglN1 and TOM20.
P Representative immunofluorescence of HIF high and HIF low breast cancer tumors from a human breast cancer microarray, and their corresponding colocalization images of EglN1 with TOM20 from a human breast cancer microarray. Nuclei were stained with DAPI (blue) (scale bar = 10 μm).
Q Scatterplots showing the correlation between co-localization of EglN1 with TOM20 and the intensity of HIF1α in different breast cancer tumors (n = 41) from a human breast cancer microarray. X-axis indicates the mean fluorescence intensity of HIF1α, and Y-axis indicates the Pearson coefficient of co-localization of EglN1 and TOM20.

Data information: Error bars in (H) represent ± SEM, *** denote P value of < 0.005 (unpaired t-test). Also See Fig EV1.
Source data are available online for this figure.

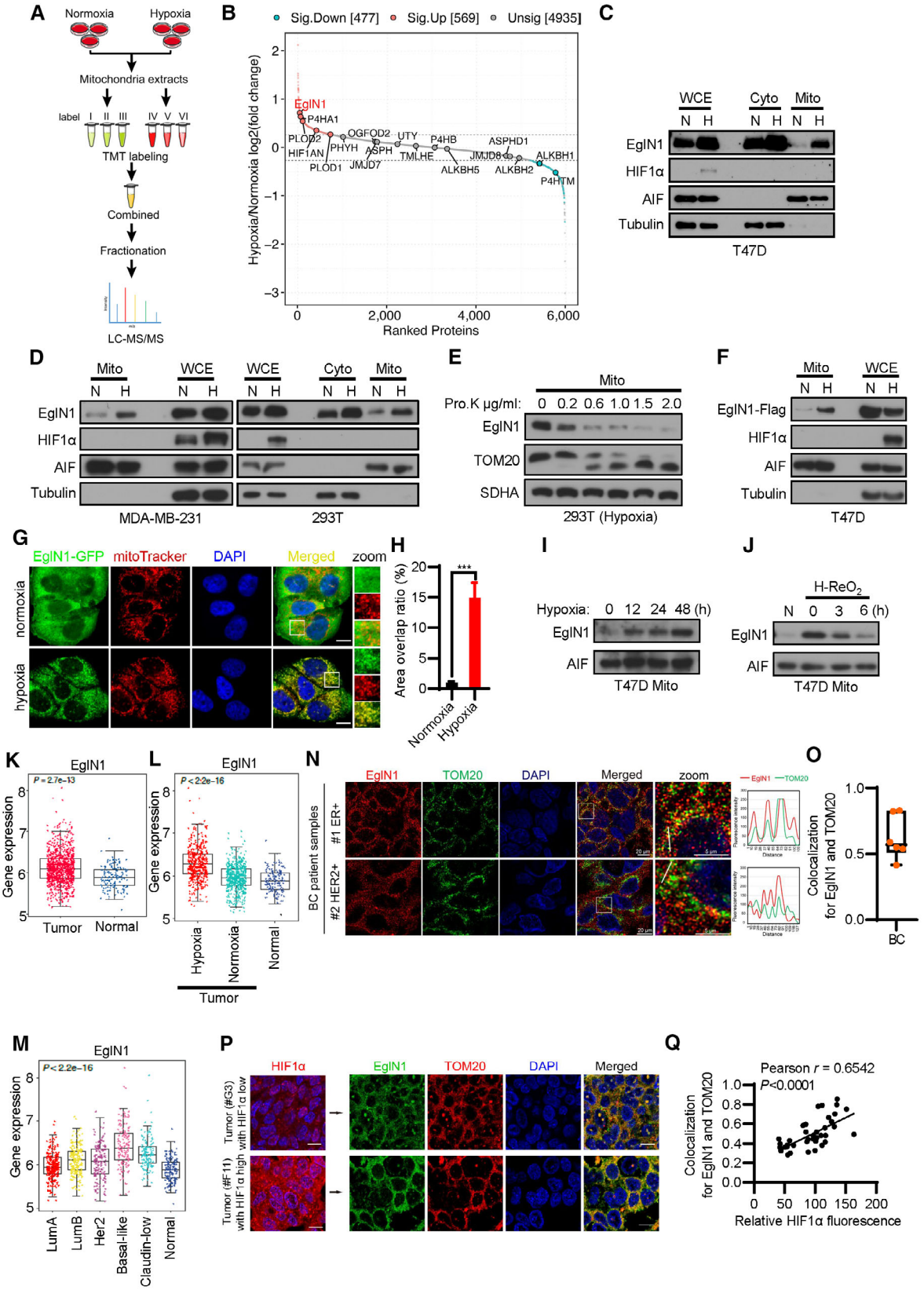
A
Normoxia
Hypoxia
Mitochondria extracts
label I II III IV V VI
TMT labeling
Combined
Fractionation
LC-MS/MS
B
Sig.Down [477] Sig.Up [569] Unsig [4935]
Hypoxia/Normoxia log2(fold change)
Ranked Proteins
EglN1
P4HA1
PLOD2
HIF1AN
PHYH
OGFOD2
ASPH
PLOD1
JMJD7
UTY
TMLHE
P4HB
ASPHD1
JMJD8
ALKBH5
ALKBH2
ALKBH1
P4HTM
C
WCE Cyto Mito
N H N H N H
EglN1
HIF1α
AIF
Tubulin
T47D
D
Mito WCE WCE Cyto Mito
EglN1
HIF1α
AIF
Tubulin
MDA-MB-231
293T
E
Mito
Pro.K μg/ml: 0 0.2 0.6 1.0 1.5 2.0
EglN1
TOM20
SDHA
293T (Hypoxia)
F
Mito WCE
EglN1-Flag
HIF1α
AIF
Tubulin
T47D
G
EglN1-GFP mitoTracker DAPI Merged zoom
normoxia
hypoxia
H
Area overlap ratio (%)
***
Normoxia Hypoxia
I
Hypoxia: 0 12 24 48 (h)
EglN1
AIF
T47D Mito
J
H-ReO2
N 0 3 6 (h)
EglN1
AIF
T47D Mito
K
EglN1
P = 2.7e-13
Gene expression
Tumor Normal
L
EglN1
P < 2.2e-16
Gene expression
Hypoxia Normoxia Normal
Tumor
N
EglN1 TOM20 DAPI Merged zoom
BC patient samples
#1 ER+
#2 HER2+
O
Colocalization for EglN1 and TOM20
BC
M
EglN1
P < 2.2e-16
Gene expression
LumA LumB Her2 Basal-like Claudin-low Normal
P
HIF1α EglN1 TOM20 DAPI Merged
Tumor (#G3) with HIF1α low
Tumor (#F11) with HIF1α high
Q
Pearson r = 0.6542
P<0.0001
Colocalization for EglN1 and TOM20
Relative HIF1α fluorescence

Figure 1.

EglN1 is a hypoxia-inducible gene (Berra *et al*, 2003), and thus hypoxia-induced transcriptional upregulation of *EglN1* could lead to its accumulation on mitochondria. To test this possibility, we generated T47D cell lines overexpressing EglN1-GFP or -Flag and examined its subcellular localization which is independent of hypoxia-mediated transcriptional regulation. The results showed that the exogenous EglN1 also accumulated on mitochondria upon hypoxia (Fig 1F). Immunofluorescence imaging showed that EglN1 was co-localized with mitochondria under hypoxia (Fig 1G and H). These data suggest that EglN1 translocates to mitochondria in response to hypoxia. Subcellular localization analyses of other EglN family members, including EglN2 and EglN3, showed that EglN2 was not localized to mitochondria, while EglN3 was downregulated on mitochondria under hypoxia, suggesting that hypoxia-induced mitochondrial accumulation is specific to EglN1 (Fig EV1E and F). Meanwhile, the mitochondrial proteomics analyses showed that an asparaginal hydroxylase HIF1AN (Hypoxia Inducible Factor 1 Subunit Alpha Inhibitor), also known as FIH (Factor Inhibiting HIF), was also accumulated on mitochondria under hypoxia (Fig 1B), and mitochondria extraction followed by Western blotting assays confirmed this conclusion (Fig EV1G). FIH acts as an oxygen sensor and asparaginal-hydroxylates HIFα for preventing the interaction of HIFα with transcriptional coactivators (Lando *et al*, 2002), the role of the accumulated FIH on mitochondria upon hypoxia warrants future investigation. Further, we found that hypoxia-induced EglN1 translocation to mitochondria was in a time-dependent manner (Fig 1I) and that reoxygenation after hypoxic treatment of these cells resulted in transfer of EglN1 away from mitochondria (Fig 1J). These collective data imply that EglN1 translocates to mitochondria in a dynamic and reversible manner, this process may signal hypoxia to mitochondria.

Furthermore, we found that EglN1 was highly expressed in breast tumor tissues, especially in tumors with the high hypoxia scores (Fig 1K and L) (Buffa *et al*, 2010; Curtis *et al*, 2012). Also, EglN1 was overexpressed in all breast cancer subtypes compared to normal tissues, with the highest expression levels in triple negative breast cancer (basal-like and claudin-low) (Fig 1M). Previous studies have reported that HIFα is readily detected in breast cancer subtypes, and increased HIFα protein levels can reflect intratumoral hypoxia in solid tumors (Briggs *et al*, 2016). We obtained six tumors from breast cancer patients including ER positive, HER2 positive and triple negative breast cancers, these samples were from the core of tumors which is considered as hypoxic region. Immunofluorescence imaging showed that EglN1 was co-localized with mitochondria in these tumor tissues (Figs 1N and O, and EV1H). Further, through immunofluorescence imaging of a human breast cancer tissue microarray, we observed that the co-localization of EglN1 with mitochondria is positively associated with the expression levels of HIF1α (Fig 1P and Q). These data indicate that the mitochondrial translocation of EglN1 may be pathologically relevant in breast cancer.

EglN1 β2β3 loop is required for its mitochondrial translocation upon hypoxia

We next sought to determine what is responsible for EglN1 mitochondrial translocation and how EglN1 translocates to mitochondria upon hypoxia. We first examined whether the translocation of EglN1 to mitochondria was regulated by its canonical oxygen sensing pathway EglN1-VHL-HIF. The EglN1 residue Pro317 is essential for its catalytic activity (Percy *et al*, 2006). Through exogenous expression of catalytically inactive EglN1 mutant (EglN1-P317R), we found that EglN1-P317R is already localized to mitochondria irrespective of oxygen concentrations, i.e., under both hypoxic and normoxic conditions (Fig 2A). We then treated cells with a potent EglN1 inhibitor IOX4, dimethyloxallyl Glycine (DMOG), desferoxamine (DFO) or ROS generator DMNQ (Gerald *et al*, 2004; Elvidge *et al*, 2006; Kohl *et al*, 2006; Lee *et al*, 2006, 2016; Murray *et al*, 2010), to chemically inhibit the hydroxylase activity of EglN1, and found that these treatments could also result in EglN1 translocation to mitochondria, similar to the effect induced by hypoxia (Fig 2B–E), suggesting that loss of EglN1 hydroxylase activity leads to its mitochondrial translocation.

VHL can recognize and bind with the prolyl-hydroxylated site of its substrate (Losman *et al*, 2020). We found that loss of VHL led to EglN1 translocation to mitochondria under normoxia (Figs 2F and

Figure 2. The EglN1 β2β3 loop is required for its mitochondrial translocation upon hypoxia.

A Immunoblots of extracts from whole cell (WCE) and mitochondria (Mito) as indicated of 293T cells transfected with EglN1-Flag WT or P317R mutant followed by treatment with normoxia (N) or hypoxia (H, 1% O_2 for 24 h).

B Immunoblots of extracts from whole cell (WCE) and mitochondria (Mito) as indicated as indicated of T47D cells treated with or without IOX4 (50 μM) for 24 h.

C Immunoblots of extracts from whole cell (WCE) and mitochondria (Mito) as indicated of T47D cells treated with normoxia (−), hypoxia (H, 1% O_2 for 24 h), DMOG (2 mM, for 24 h), or DFO (200 μM, for 12 h).

D, E Immunoblots of extracts from whole cell (WCE) and mitochondria (Mito) of 293T cells transfected with EglN1-Flag (D) or T47D (E) cells followed by treatment with normoxia (−), hypoxia (H, 1% O_2 for 24 h), DMOG (2 mM, for 24 h), or DFO (200 μM, for 12 h).

F Immunoblots of extracts from whole cell (WCE) and mitochondria (Mito) of T47D cells infected with EglN1-Flag followed by another infection with control sgRNA (−) or VHL sgRNA (sgVHL) under treatment with normoxia (N) or hypoxia (H, 1% O_2 for 24 h).

G Immunoblots of extracts from whole cell (WCE) and mitochondria (Mito) as indicated of 786-O cells treated with normoxia (N) or hypoxia (H, 1% O_2 for 24 h).

H Immunoblots of extracts from whole cell (WCE) and mitochondria (Mito) as indicated of 786-O cells infected with control vector (−) or HA-VHL.

I A schematic illustration of EglN1 β2β3 loop (241–251) for substrate binding.

J Immunoblots of extracts from whole cell (WCE) and mitochondria (Mito) as indicated of T47D cells infected with control EglN1-WT-Flag or EglN1-▵β2β3-Flag followed by infection with EglN1 sh1045 with or without hypoxia (1% O_2) treatment for 24 h.

K Immunofluorescence of T47D cells infected with EglN1-GFP or EglN1-▵β2β3-GFP followed by treatment with hypoxia (1% O_2 for 24 h) and with MitoTracker Red staining for 15 min. Nuclei were stained with DAPI (blue) (scale bar = 10 μm).

L Quantification data of each cells' area overlap ratio for co-localization of EglN1-GFP and mitochondria from (K) (N = 6 images in total).

Data information: Error bars in (L) represent ± SEM, *** denote P value of 0.005 (unpaired t-test). Also See Fig EV2.
Source data are available online for this figure.

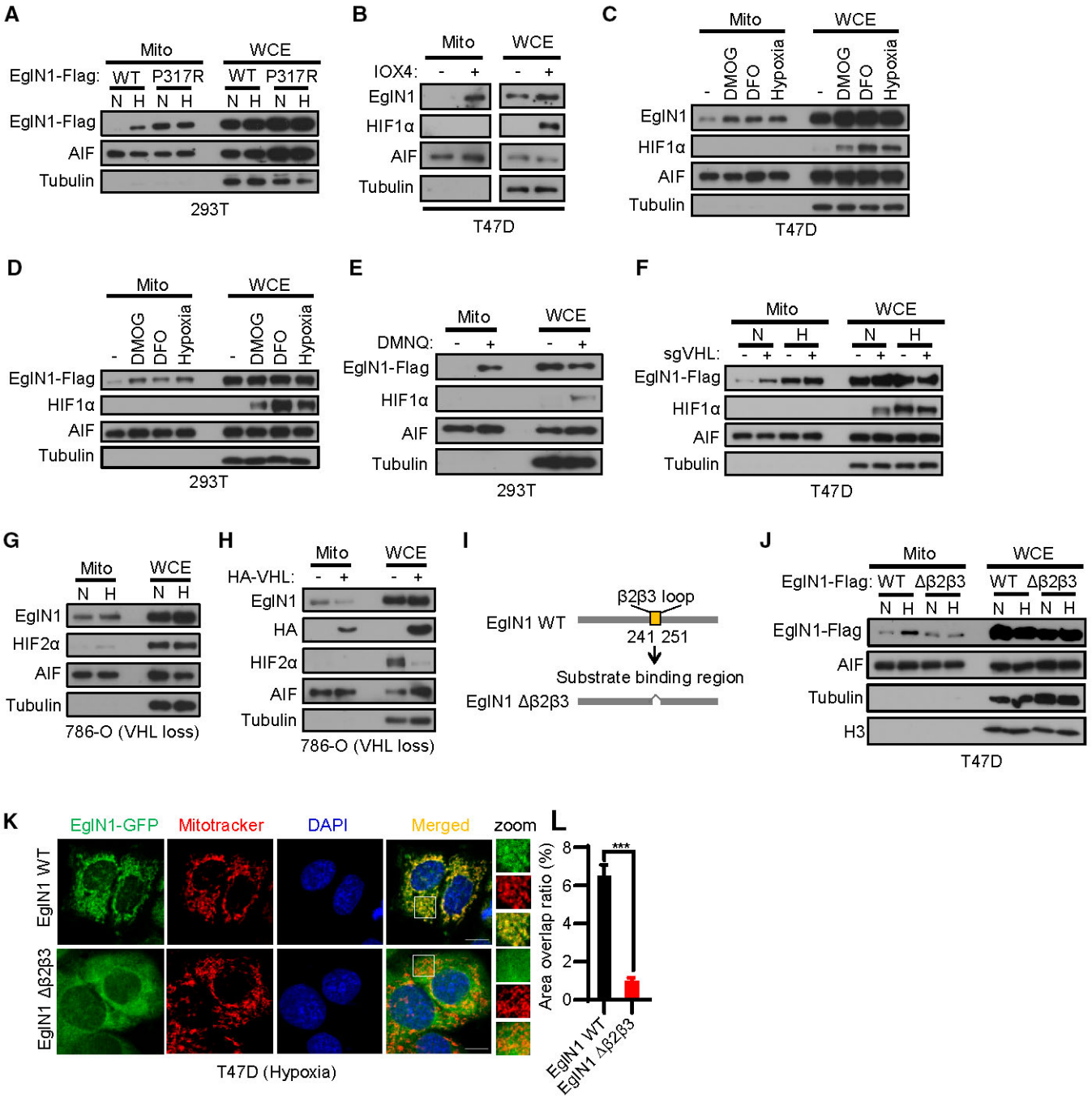

Figure 2.

EV2A). And, EglN1 was already accumulated on mitochondria under normoxia in 786-O cells with naturally loss of VHL function (Zhang *et al*, 2018), hypoxia treatment failed to further promote its translocation to mitochondria (Fig 2G), indicating hypoxia-induced mitochondrial translocation of EglN1 is through VHL. Reconstitution with VHL, which was also localized to mitochondria, could decrease the expression levels of EglN1 on mitochondria (Fig 2H). These data suggest that Loss of VHL results in the mitochondrial translocation of EglN1.

Our data showed that hypoxia, inhibition of EglN1 prolyl hydroxylase activity, or VHL loss could result in EglN1 translocation to mitochondria, we hypothesized that an EglN1 substrate may be present on mitochondria, given that prolyl hydroxylation is a transient reaction and the enzyme-substrate interactions are barely detectable under normoxia, while the interactions of EglN1 with its substrate can be trapped and sequentially accumulated under conditions such as hypoxia, lacking of EglN1 hydroxylase activity, or loss of VHL (Zurlo *et al*, 2019), if so, deletion of EglN1 substrate binding region

would inhibit its mitochondrial accumulation upon hypoxia. To test this possibility, we deleted the EglN1 β2β3 loop which is well-established as responsible for EglN1 substrate binding (Fig 2I) (Flashman *et al*, 2008; Chowdhury *et al*, 2009), and our data showed that EglN1 with loss of β2β3 loop (EglN1-△β2β3) failed to respond to hypoxia for its mitochondrial translocation, and its expression on mitochondria was significantly lower than that of EglN1-WT (Fig 2J). Consistently, immunofluorescence imaging showed that EglN1-△β2β3, unlike EglN1-WT, was barely co-localized with mitochondria under hypoxia (Fig 2K and L). These data suggest that the mitochondrial translocation of EglN1 upon hypoxia is through its β2β3 loop region and an EglN1 substrate is potentially present on mitochondria.

Previous data suggest that hypoxia, loss of the EglN1 hydroxylase activity, or lacking VHL can lead to accumulated interactions of EglN1 with HIFα in nucleus where EglN1 hydroxylates HIFα under sufficient oxygen conditions (Groulx & Lee, 2002; Wotzlaw *et al*, 2010; Pientka *et al*, 2012). We found that EglN1 with loss of β2β3 loop (EglN1-△β2β3) did not affect its expression levels in nucleus (Fig EV2B), suggesting that the nuclear translocation of EglN1 is independent of its β2β3 loop region. We reason that EglN1 nuclear localization signal (NLS) is primarily responsible for its nuclear translocation (Pientka *et al*, 2012). We further examined the effect of HIF on the mitochondrial translocation of EglN1. Our data showed that either HIF1α or HIF2α was barely localized to mitochondria (Fig 2B–H), and inhibition of the HIF pathway either by HIF1β depletion or by treatment with HIF2α inhibitor PT2399 had no effect on the mitochondrial translocation of EglN1 (Fig EV2C and D), suggesting that EglN1 translocation to mitochondria is independent of HIF. Altogether, we demonstrate that EglN1 translocates to mitochondria upon hypoxia through its substrate binding region β2β3 loop in a HIF-independent manner.

Mitochondrial EglN1 contributes to breast tumor growth

We next examined the effect of mitochondrial EglN1 on tumor cell growth under hypoxia. We observed that EglN1 depletion in T47D or MDA-MB-231 cell lines inhibited tumor cell proliferation under normoxia and hypoxia (Fig EV3A–F). Furthermore, through *in vivo* study, we found that overexpression of EglN1 could promote the tumor cell growth (Fig EV3G–J). Consistently, depletion of EglN1 inhibited the tumor cell growth, and overexpression of EglN1 in the EglN1-depleted cells could restore the tumor growth with its higher growth rate than that of the control shRNA cells (Fig EV3K–N). Therefore, we investigated the effect of mitochondrial EglN1 on tumor growth by comparing with EglN1-WT as positive control and control vector as negative control in the EglN1-depleted cells in the following *in vivo* study. We found that EglN1-△β2β3, which loses the ability for mitochondrial translocation in response to hypoxia, failed to rescue the cell growth defects caused by EglN1 depletion under normoxia and hypoxia (Figs 3A–F and EV3O). Further, we orthotopically injected EglN1-depleted MDA-MB-231 cells expressing control vector (Ctrl), EglN1-△β2β3, or EglN1-WT into the mammary fat pads of nude mice and monitored tumor growth every third day by caliper, and observed that EglN1-△β2β3, unlike EglN1-WT, failed to restore breast cancer progression in EglN1-depleted cells *in vivo* (Fig 3G–I), suggesting that EglN1 β2β3 loop is required for tumor cell growth.

Our above data showed that EglN1 is localized to the mitochondrial outer membrane, we therefore generated a TOM20-EglN1-Flag construct to anchor EglN1 to the mitochondrial outer membrane (Fig EV3P), since mitochondrial protein TOM20 is known to reside on the mitochondrial outer membrane and our data showed that overexpression of TOM20 had no effect on breast tumor cell growth (Fig EV3Q–T). We found that reconstitution of TOM20-EglN1, similar to EglN1-WT, could rescue EglN1 depletion-mediated defects in tumor cell growth under normoxia and hypoxia (Figs 3J–O and EV3U). To further examine the function of mitochondrial EglN1 in breast cancer progression *in vivo*, we also orthotopically injected EglN1-depleted MDA-MB-231 cells expressing control vector (Ctrl), TOM20-EglN1, or EglN1-WT into the mammary fat pads of nude mice and monitored tumor growth every third day by caliper. Consistent with the *in vitro* phenotypes, TOM20-EglN1, similar to EglN1-WT, could restore breast cancer progression in EglN1-depleted cells (Fig 3P–R). Taken together, these data suggest that mitochondrial EglN1 contributes to tumor cell growth *in vitro* and *in vivo*.

Consistent with the above data showing that HIF has no effect on mitochondrial translocation of EglN1, inhibition of the HIF pathway by PT2399 treatment also did not affect EglN1 regulation of breast cancer cell growth (Fig EV3V and W). Then, we further determined the mechanism of how mitochondrial EglN1 regulates cancer cell growth.

EglN1 prolyl-hydroxylates AMPKα on mitochondria

In light of our above data suggesting that an EglN1 substrate might be present on mitochondria responsible for the EglN1

Figure 3. Mitochondrial EglN1 contributes to breast cancer progression.

A–F Immunoblots of cell lysates (A, D), MTT assays (B, E), and 2D colony formation assays (C, F) from T47D or MDA-MB-231 cell lines infected with control vector (Ctrl), EglN1-WT-Flag, or EglN1-△β2β3-Flag followed by infection with control shRNA (shCtrl) or EglN1 sh1045 (EglN1 shRNA) under hypoxic (1% O_2) condition.

G–I Mouse xenograft experiments were performed with the cells generated in (D). Tumor growth curves (G) and tumor weights (H) were calculated, and gross tumors (I) were presented (n = 6 mice per group).

J–O Immunoblots of cell lysates (J, M), MTT assays (K, N), and 2D colony formation assays (L, O) from T47D or MDA-MB-231 cell lines infected with control vector (Ctrl), EglN1-Flag, or TOM20-EglN1-Flag followed by infection with control shRNA (shCtrl) or EglN1 sh1045 (EglN1 shRNA) under hypoxic (1% O_2) condition.

P–R Mouse xenograft experiments were performed with the cells generated in (m). Tumor growth curves (P) and tumor weights (Q) were calculated, and gross tumors (R) were presented (n = 6 mice per group).

Data information: Error bars in (B, E, G, H, K, N, P, Q) represent ± SEM, ** and *** denote P value of < 0.01, and 0.005, respectively, and ns denotes not significant (unpaired t-test). n = 3 independent technical replicate experiments for MTT assays. Also See Fig EV3.
Source data are available online for this figure.

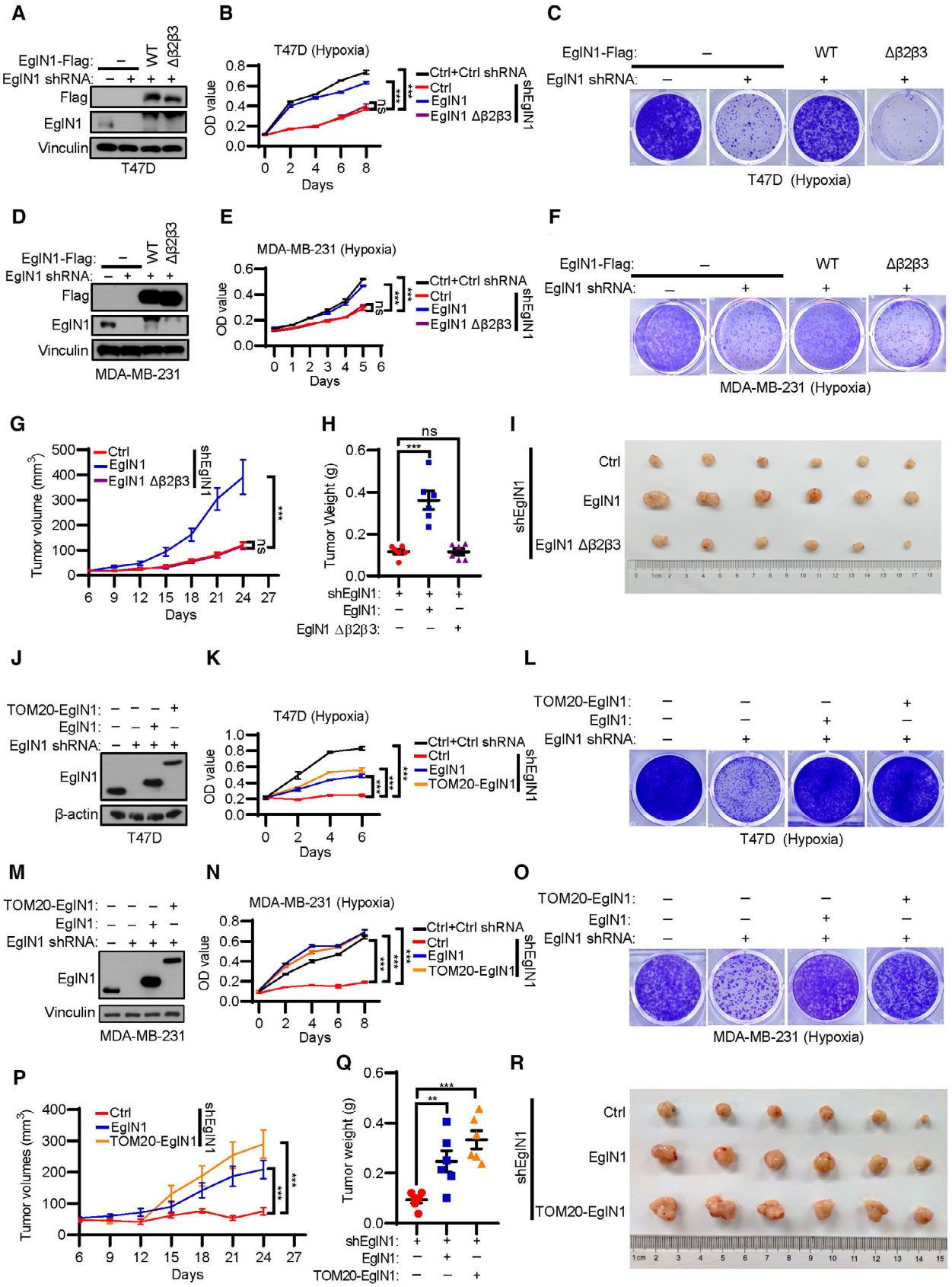

Figure 3.

mitochondrial translocation, we therefore sought to identify the possible substrate of mitochondrial EglN1. We performed EglN1 immunoprecipitation-mass spectrometry (IP-MS) in T47D cells under normoxia versus hypoxia (Fig 4A), where hypoxia could potentially trap the enzyme-substrate interactions. Through integrated analyses of IP-MS and mitochondrial proteomics, we found that AMPKα1 was localized to mitochondria and meanwhile specifically interacted with EglN1 under hypoxia (Fig 4B). It has been reported that hypoxia-activated phosphorylation of AMPKα is an essential regulatory step to support continued cell proliferation during hypoxic stress via restoring metabolic homeostasis (Lee *et al*, 2020b). However, the direct link of oxygen sensing to AMPKα phosphorylation activation has not been documented. Consistent with previous studies, we observed that hypoxia induced the phosphorylation of AMPKα in T47D and MBA-MB-231 cell lines (Fig EV4A and B). We wondered whether EglN1 could hydroxylate AMPKα to control its phosphorylation. AMPKα includes two isoforms, AMPKα1 and AMPKα2, they share the identical sequence within their respective kinase domains for phosphorylation (AMPKα1 at Thr183 and AMPKα2 at Thr172) (Trefts & Shaw, 2021). Co-immunoprecipitation (Co-IP) assays showed that EglN1 could interact with both AMPKα1 and AMPKα2 during hypoxia (Fig 4C), glutathione *S*-transferase (GST) pull-down assay also showed that EglN1 interacted with both AMPKα1 and AMPKα2 (Fig 4D). We therefore examined both AMPKα1 and AMPKα2 as potential EglN1 substrates.

We used anti-AMPKα antibody recognizing both AMPKα1 and AMPKα2 and confirmed that AMPKα specifically interacted with EglN1 under hypoxia in T47D and MBA-MB-231 cells, as did HIF1α (Figs 4E and EV4C). VHL loss also induced EglN1-AMPKα interaction, with increased phosphorylation levels of AMPKα (Fig EV4D and E). Subcellular fractionation followed by Co-IP assays showed that the AMPKα-EglN1 interaction took place on mitochondria, not in cytosol or nucleus (Fig 4F). Furthermore, we also observed that EglN1 interacted with phosphorylated form of AMPKα under hypoxia (Fig 4G). Compound C, which inhibits AMPK phosphorylation activation (Zhou *et al*, 2001), blocked the interaction of EglN1 with either phosphorylated-AMPKα or total AMPKα (Fig 4G), suggesting that AMPKα phosphorylation is essential for the EglN1-AMPKα interaction. Furthermore, we found that phosphorylated-AMPKα barely interacted with EglN1-△β2β3, as did HIF1α (Fig 4H), suggesting that EglN1 interacted with phosphorylated-AMPKα through its β2β3 loop region.

To further determine that AMPKα could be prolyl-hydroxylated by EglN1, we performed liquid chromatography–tandem mass spectrometry (LC–MS/MS) in 786-O cells treated with or without DMOG to identify their potential prolyl-hydroxylation sites (Fig EV4F) (Zhang *et al*, 2018). We found that prolines 188 and 177, in their

Figure 4. EglN1 prolyl-hydroxylates AMPKα on mitochondria.

A Schematic representation of strategy for identification of EglN1-interacting proteins in T47D cells exposed to hypoxia (1% O2 for 24 h) versus normoxia by mass spectrometry.
B Sequence coverage values of EglN1, AMPKα1, and HIF1α from mass spectrometry analysis.
C Immunoblots (IB) of whole cell extracts (WCE) and immunoprecipitations (IP) of T47D cells infected with control vector, AMPKα1-Flag, or AMPKα2-Flag followed by treatment with normoxia or hypoxia (1% O_2) for 24 h.
D Immunoblots (IB) of proteins from *in vitro* translation or recombinant protein purification (input). *In vitro* immunoprecipitation (IP) analyses for protein interactions between recombinant GST-EglN1 and AMPKα1-Flag or AMPKα2-Flag, respectively.
E Immunoblots (IB) of whole cell extracts (WCE) and immunoprecipitations (IP) of T47D cells infected with control vector or EglN1-Flag followed by treatment with normoxia or hypoxia (1% O_2) for 24 h.
F Immunoblots of extracts from cytosol (Cyto), mitochondria (Mito) and nucleus, and their respective immunoprecipitations (IP) from T47D mitochondrial extraction generated in Fig 1F.
G Immunoblots (IB) of whole cell extracts (WCE) and immunoprecipitations (IP) of T47D cells infected with control vector or EglN1-Flag followed by treatment with or without compound C (Comp C, 10 μM) for 24 h under hypoxic condition.
H Immunoblots (IB) of whole cell extracts (WCE) and immunoprecipitations (IP) of T47D cells infected with control vector, EglN1-WT-Flag, or EglN1-△β2β3-Flag.
I A schematic illustration of highly conserved sequences for prolyl hydroxylation within kinase domains (KD) of AMPKα1 and AMPKα2. Those prolines for hydroxylation were highlighted in red.
J Immunoblots of lysates from T47D and 786-O cells treated with or without hypoxia (1% O_2) for 24 h.
K Immunoblots of lysates from T47D and 786-O cells treated with or without DMOG (2 mM) for 24 h.
L Immunoblots of lysates from 293T cells transfected with AMPKα1-WT/P188A-Flag or AMPKα2-WT/P177A-Flag, respectively.
M Immunoblots of lysates from T47D and 786-O cells infected with control shRNA or EglN1 shRNA.
N Immunoblots of lysates from T47D cells infected with control vector (−), EglN1-WT, or EglN1-P317R followed by infection with control shRNA (−) or EglN1 sh1045 (EglN1 shRNA).
O Immunoblots of lysates from T47D cells infected with control vector (−), EglN1-WT, or EglN1-△β2β3 followed by infection with control shRNA (−) or EglN1 sh1045 (EglN1 shRNA).
P *In vitro* hydroxylation assays were performed through purified GST-EglN1 WT or P317R mutant incubated with AMPKα1-biotinylated synthetic peptides followed by dot immunoblot analyses with anti-AMPKα-Pro188-OH antibody.
Q Indicated peptides were incubated with whole cell lysates from 293T cells transfected with HA-VHL, and precipitated with streptavidin. Immunoblot assays of those whole cell lysates and precipitated proteins with HA antibody, dot blot assays of the indicated peptides with biotin.
R Immunoblots (IB) of whole cell extracts (WCE) and immunoprecipitations (IP) of 786-O cells infected with control vector or HA-VHL followed by treatment with or without DMOG (2 mM) for 24 h.
S Immunoblots of lysates from 786-O cells infected with control vector or HA-VHL followed by treatment with or without DMOG (2 mM) for 24 h.
T Immunoblots of lysates from 786-O cells expressing HA-VHL infected with control vector (−), EglN1-WT, or EglN1-P317R followed by infection with control shRNA (−) or EglN1 sh1045 (EglN1 shRNA).
U A proposed model depicting the regulatory mechanism of mitochondrial EglN1 under normoxia.

Data information: Also See Fig EV4.
Source data are available online for this figure.

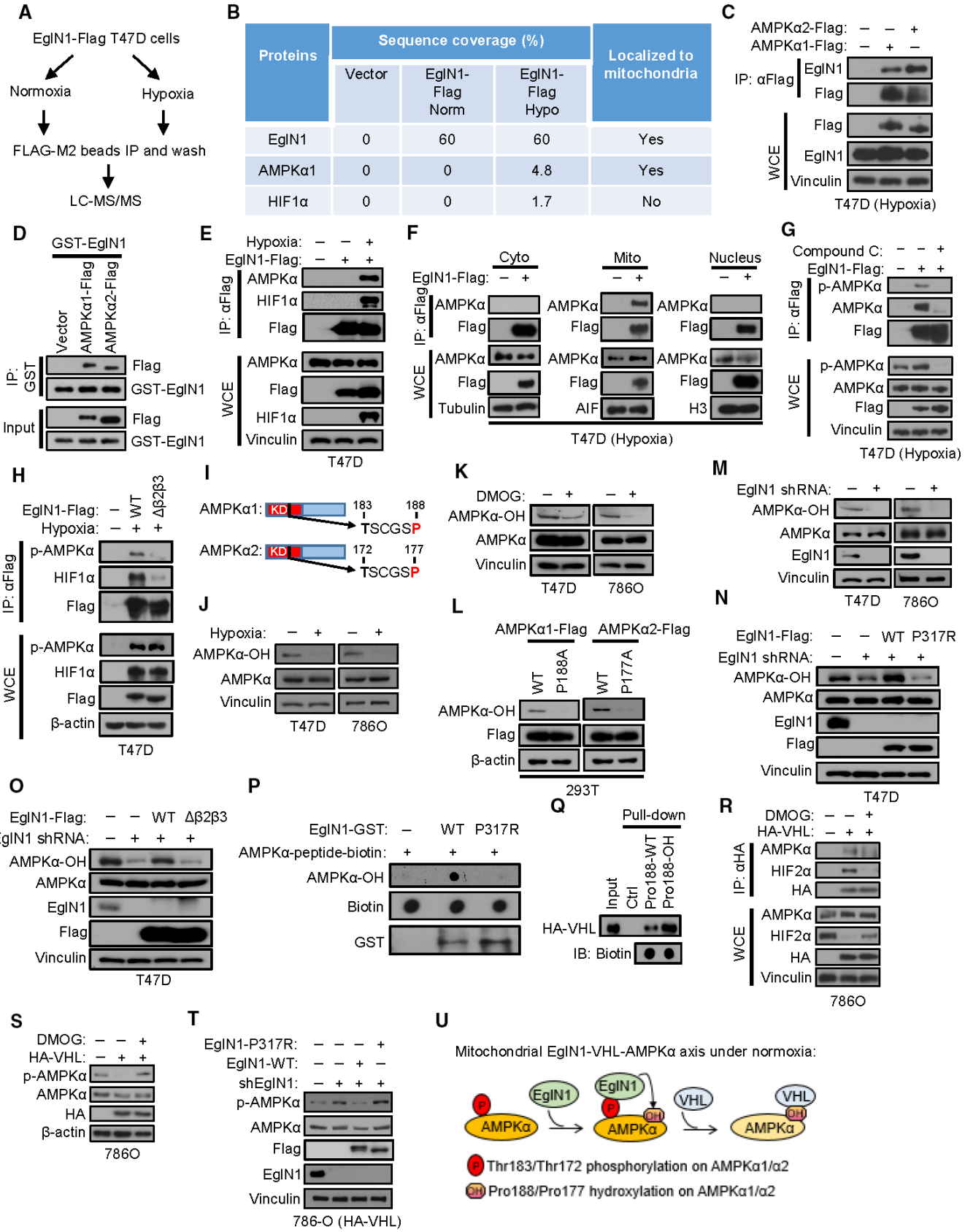
A
EglN1-Flag T47D cells
Normoxia
Hypoxia
FLAG-M2 beads IP and wash
LC-MS/MS
B
Proteins
Sequence coverage (%)
Vector
EglN1-Flag Norm
EglN1-Flag Hypo
Localized to mitochondria
EglN1 0 60 60 Yes
AMPKα1 0 0 4.8 Yes
HIF1α 0 0 1.7 No
C
AMPKα2-Flag:
AMPKα1-Flag:
IP: αFlag
EglN1
Flag
WCE
Vinculin
T47D (Hypoxia)
D
GST-EglN1
Vector
AMPKα1-Flag
AMPKα2-Flag
IP: GST
Input
GST-EglN1
E
Hypoxia:
EglN1-Flag:
IP: αFlag
AMPKα
HIF1α
Flag
WCE
Vinculin
T47D
F
Cyto
Mito
Nucleus
AIF
H3
Tubulin
T47D (Hypoxia)
G
Compound C:
p-AMPKα
T47D (Hypoxia)
H
EglN1-Flag:
WT
Δβ2β3
Hypoxia:
p-AMPKα
HIF1α
Flag
β-actin
T47D
I
AMPKα1:
AMPKα2:
KD
183
188
172
177
TSCGSP
J
Hypoxia:
AMPKα-OH
T47D
786O
K
DMOG:
AMPKα-OH
M
EglN1 shRNA:
L
AMPKα1-Flag
AMPKα2-Flag
P188A
P177A
293T
N
EglN1-Flag:
WT
P317R
O
Δβ2β3
P
EglN1-GST:
AMPKα-peptide-biotin:
Biotin
GST
Q
Pull-down
Input
Ctrl
Pro188-WT
Pro188-OH
HA-VHL
IB: Biotin
R
HA-VHL:
IP: αHA
HIF2α
HA
S
786O
T
EglN1-P317R:
EglN1-WT:
shEglN1:
786-O (HA-VHL)
U
Mitochondrial EglN1-VHL-AMPKα axis under normoxia:
Thr183/Thr172 phosphorylation on AMPKα1/α2
Pro188/Pro177 hydroxylation on AMPKα1/α2

Figure 4.

respective conserved kinase domains of AMPKα1 and AMPKα2, were hydroxylated in those untreated cells, and their hydroxylation could be inhibited by hydroxylase inhibitor DMOG (Fig EV4G–I). Interestingly, we found that these hydroxylated prolyl-residues are located in their highly conserved kinase domain regions close to their respective phosphorylation sites (Fig 4I). To study the AMPKα hydroxylation sites in cells, we generated an antibody to recognize AMPKα-Pro188/177 hydroxylation (AMPKα-OH), and we observed that recognition of AMPKα by the AMPKα-OH antibody was significantly decreased in cells under DMOG or hypoxia treatment (Fig 4J and K). And, AMPKα-OH antibody failed to recognize AMPKα1 P188A or AMPKα2 P177A mutants (Fig 4L). The expression level of AMPKα-OH recognized by AMPKα-OH antibody was decreased in AMPKα1-depleted cells, suggesting the specificity of this antibody for AMPKα (Fig EV4J). Moreover, we found that EglN1 depletion inhibited the prolyl-hydroxylation of AMPKα (Fig 4M), and this regulation depends on its catalytic activity and β2β3 loop region (Fig 4N and O). Through *in vitro* hydroxylation assays with recombinant EglN1 and AMPKα peptide, we observed that EglN1-WT, but not EglN1 catalytically inactive mutant EglN1-P317R, could directly hydroxylate AMPKα peptide (Fig 4P). Consistent with the IP assays showing that EglN1 interacted with phosphorylated-AMPKα (Fig 4G), AMPKα WT, but not AMPKα T183A mutant, can be hydroxylated (Fig EV4K). Altogether, these data suggest that EglN1 prolyl-hydroxylates phosphorylated-AMPKα at Pro188/177.

We performed *in vitro* binding assays with biotinylated AMPKα-derived peptides that span the AMPKα hydroxylation site (Fig EV4L) and found that VHL preferentially bound to hydroxylated AMPKα-derived peptide (Fig 4Q). VHL could interact with AMPKα, and treatment with DMOG decreased their interaction in 786-O cells (Fig 4R), suggesting that VHL interacts with AMPKα in a prolyl-hydroxylation-dependent manner. Reconstitution of HA-VHL in 786-O cells decreased AMPKα phosphorylation, and treatment with DMOG restored its phosphorylation (Fig 4S). EglN1 depletion in VHL-reconstituted 786-O cells increased AMPKα phosphorylation, while this upregulated phosphorylation could be reversed by overexpression EglN1-WT, but not hydroxylase-inactivated EglN1-P317R mutant (Fig 4T). These data suggest that VHL can recognize EglN1-catalyzed prolyl-hydroxylation of AMPKα for limiting AMPKα phosphorylation (Fig 4U).

Hypoxia-induced mitochondrial translocation of EglN1-AMPKα activates the AMPK pathway

To examine whether the hypoxia-induced EglN1-AMPKα interaction is responsible for EglN1 mitochondrial translocation, we first performed mitochondrial extraction under hypoxia versus normoxia to test their protein levels on mitochondria. We found that both AMPKα1 and AMPKα2, similar to EglN1, could translocate to mitochondria upon hypoxia (Fig EV5A). Through proteinase K digestion of isolated mitochondria, we found that AMPKα also translocated to the mitochondrial outer membrane upon hypoxia, similar to EglN1 (Fig 5A). Compound C, which inhibits the EglN1-AMPKα interaction, not only inhibited the expression of phosphorylated-AMPKα and total AMPKα on mitochondria, but also decreased the mitochondrial translocation of EglN1 (Fig 5B), suggesting that AMPKα phosphorylation activation is required for the mitochondrial translocation of both EglN1 and AMPKα. Indeed, similar to EglN1, phosphorylated-AMPKα was also co-localized with mitochondria in tumor tissues from breast cancer patients (Figs 5C and EV5B). On the other hand, EglN1 depletion also downregulated the mitochondrial translocation of AMPKα, and EglN1-△β2β3, which loses the interaction with phosphorylated-AMPKα, failed to rescue EglN1 depletion-mediated decrease in the mitochondrial translocation of AMPKα (Fig 5D), suggesting that EglN1 β2β3 loop region is not only required for EglN1 mitochondrial translocation, but also essential for the translocation of AMPKα to mitochondria. These data suggest that the hypoxia-induced

Figure 5. Hypoxia-induced mitochondrial translocation of EglN1-AMPKα activates the AMPK pathway.

A Immunoblots of mitochondrial extracts (Mito) treated with or without Proteinase K (2 μg/ml) and whole cell extracts (WCE) from T47D cells under normoxic (N) or hypoxic (H, 1% O_2 for 24 h) conditions.

B Immunoblots of mitochondrial extracts (Mito) and whole cell extracts (WCE) from T47D treated with or without compound C (Comp C, 10 μM for 24 h) under hypoxia.

C Representative immunofluorescence of p-AMPKα and TOM20 with tumor tissues from breast cancer patients. The right panel showed the quantification of fluorescence intensity of TOM20 and p-AMPKα along the line in merged image.

D Immunoblots of mitochondrial extracts (Mito) and whole cell extracts (WCE) from T47D cells infected with control vector (Ctrl), EglN1-WT-Flag, or EglN1-△β2β3-Flag followed by infection with control shRNA (shCtrl) or EglN1 sh1045 (EglN1 shRNA) under hypoxic (1% O_2) condition for 24 h.

E Immunoblots of cell lysates from T47D or MDA-MB-231 cell lines infected with control vector (Ctrl), EglN1-WT-Flag, or EglN1-△β2β3-Flag followed by infection with control shRNA (shCtrl) or EglN1 sh1045 (EglN1 shRNA) under hypoxic (1% O_2) condition for 24 h.

F Immunoblots assays of MDA-MB-231 xenograft tumors from Fig 3I (EglN1 WT and EglN1 Δβ2β3).

G Immunoblots of cell lysates from MDA-MB-231 cell lines generated in (E).

H, I Representative fluorescence imaging (N = 30 images in total) (H) and corresponding quantification data (I) in GFP-LC3 stably expressed MDA-MB-231 cell lines generated in (E) treated with hypoxia (1% O_2 for 24 h). (scale bar = 10 μm).

J, K Representative fluorescence imaging (N = 6 images in total) of lipid droplets stained with Nile Red (J) and corresponding quantification data (K) in MDA-MB-231 cell lines generated in (E) treated with hypoxia (1% O_2 for 24 h). Nuclei were stained with DAPI (blue) (scale bar = 10 μm).

L Immunoblots of cell lysates from MDA-MB-231 cells infected with control vector (Ctrl), EglN1-WT-Flag, or TOM20-EglN1-WT-Flag followed by infection with control shRNA (shCtrl) or EglN1 sh1045 (EglN1 shRNA) under hypoxic (1% O_2) condition for 24 h.

M, N Representative fluorescence imaging (N = 30 images in total) (M) and corresponding quantification data (N) in GFP-LC3 stably expressed MDA-MB-231 cell lines generated in (L) treated with hypoxia (1% O_2 for 24 h). (scale bar = 10 μm).

O, P Representative fluorescence imaging (N = 6 images in total) of lipid droplets stained with Nile Red (O) and corresponding quantification data (P) in MBA-MB-231 cell lines generated in (L) treated with hypoxia (1% O_2 for 24 h). Nuclei were stained with DAPI (blue) (scale bar = 20 μm).

Data information: Error bars in (I, K, N, P) represent ± SEM, *** denotes P value of 0.005 and ns denotes not significant (unpaired t-test). Also See Fig EV5.
Source data are available online for this figure.

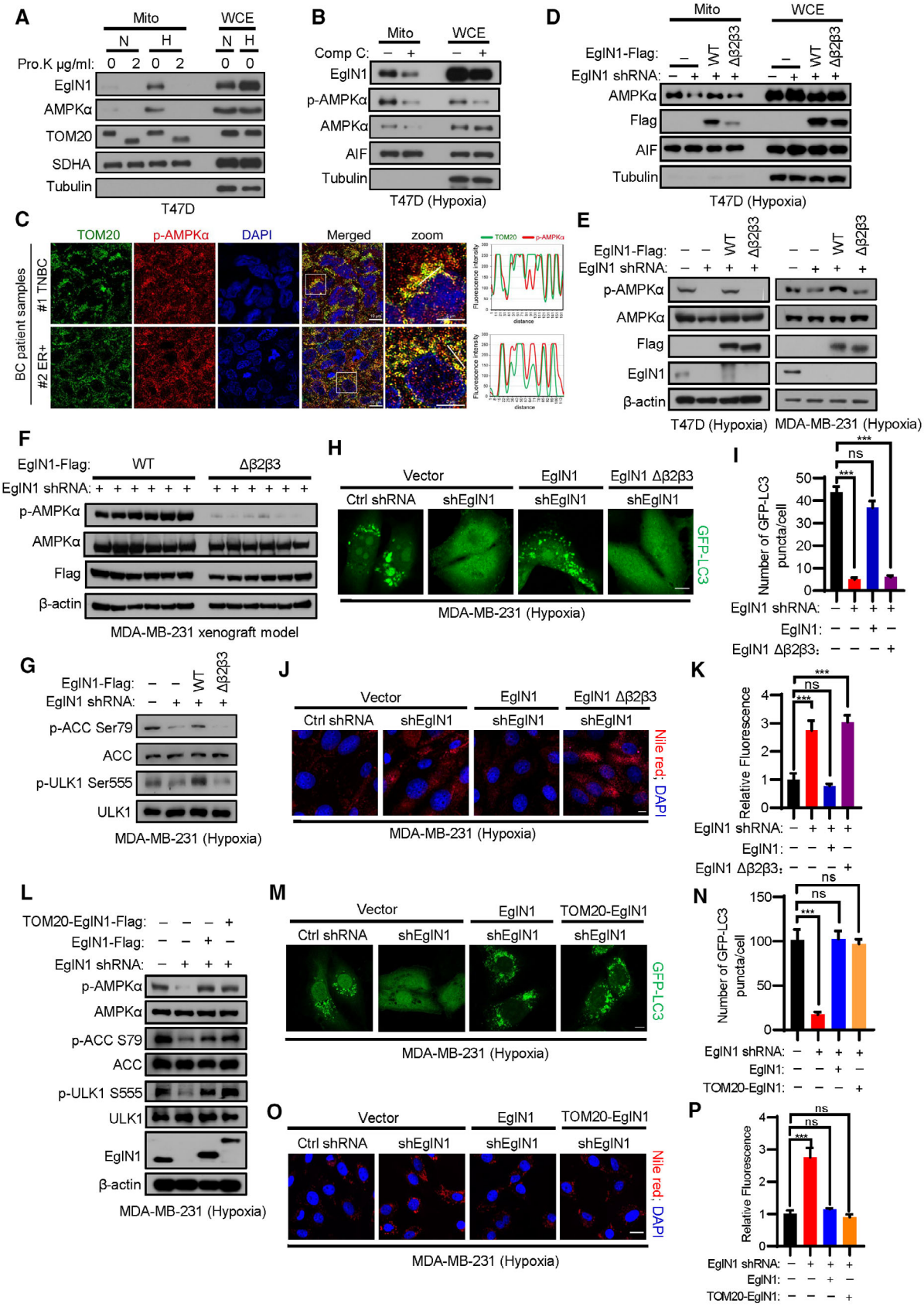

Figure 5.

EglN1-AMPKα interaction is responsible for their mutual mitochondrial translocation.

AMPKα phosphorylation leads to increased catabolism (e.g., autophagy) and decreased anabolism (*e.g.*, lipid synthesis) for restoring metabolic homeostasis under metabolic stresses (Lee *et al*, 2020b). However, whether hypoxia-induced mitochondrial translocation of AMPKα contributes to AMPKα phosphorylation activation is unknown. Therefore, we sought to determine whether EglN1 regulation of AMPKα mitochondrial translocation affects AMPKα phosphorylation. The Western blotting showed that EglN1 depletion inhibited AMPKα phosphorylation under hypoxia as well as in MDA-MB-231 xenograft tumors (Figs 5E and EV5C), EglN1-△β2β3, unlike EglN1-WT, failed to reverse the decreased phosphorylation of AMPKα (Fig 5E and F). In line with the functions of AMPKα, EglN1 depletion decreased the phosphorylation levels of AMPKα downstream substrates ULK1 and ACC (Fig 5G), both of which have been reported to reside on mitochondria and their phosphorylation activations mark increased autophagy and decreased lipid synthesis, respectively (Trefts & Shaw, 2021). Consistently, Western blotting assays showed that EglN1 KD reduced LC3-II levels with or without CQ treatment under hypoxia (Fig EV5D), fluorescence imaging showed that EglN1 depletion inhibited the GFP-LC3-II puncta during hypoxia (Fig 5H and I). Through fluorescence imaging of Nile Red stained cells, we observed that EglN1 depletion increased lipid synthesis under hypoxia (Fig 5J and K). EglN1-△β2β3, unlike EglN1-WT, failed to reverse these changes caused by EglN1 depletion (Fig 5G–K), which is consistent with the effect of EglN1 on AMPKα phosphorylation. These data suggest that the EglN1 β2β3 region plays an essential role in restoring metabolic homeostasis under hypoxia.

On the other hand, we found that TOM20-EglN1, similar to EglN1-WT, could reverse the decreased phosphorylation levels of AMPKα, ULK1 and ACC caused by EglN1 depletion (Fig 5L), and also could reverse the EglN1-depletion induced decrease in GFP-LC3-II puncta and increase in lipid synthesis (Fig 5M–P). Collectively, these data suggest that mitochondrial EglN1 activates the AMPK pathway and plays an essential role in restoring metabolic homeostasis under hypoxic stress.

EglN1 recruiting CaMKK2 to AMPKα under hypoxia contributes to breast tumor growth

We then determined how the accumulated EglN1-AMPKα interaction activates AMPKα phosphorylation. Previous work has shown that hypoxia-induced AMPKα phosphorylation is mediated by CaMKK2 (Gusarova *et al*, 2011). Co-IP assays showed that EglN1 could interact with CaMKK2, AMPKγ1 and AMPKβ1 on mitochondria under hypoxia, but barely interacted with LKB1 (Fig 6A). Therefore, we hypothesized that EglN1 could work as a scaffold protein linking CaMKK2 to AMPKα. Indeed, AMPKα showed stronger interaction with CaMKK2 under hypoxia and was substantially phosphorylated, both of which were significantly inhibited by EglN1 depletion (Fig 6B), indicating that EglN1 recruits CaMKK2 to AMPKα under hypoxia for AMPKα phosphorylation.

We next sought to determine whether EglN1-regulated tumor cell growth acts through the AMPK pathway. We found that overexpression of the constitutively active AMPKα-T172D mutant alone could promote tumor cell proliferation (Fig EV5E and F), and inhibition of the AMPK pathway by depletion of AMPKα or AMPKα phosphorylation inhibitor compound C treatment led to decreased breast cancer cell growth under normoxia and hypoxia (Fig EV5G–K), suggesting that AMPK is essential for breast cancer cell growth. Then, we examined whether AMPKα phosphorylation activation could rescue the EglN1 depletion-mediated effect on tumor cell growth. Our data showed that overexpression of AMPKα-T172D mutant could rescue tumor growth defect caused by EglN1 depletion *in vitro* and *in vivo* (Figs 6C–G and EV5L). These data suggest that EglN1 regulation of tumor cell growth is at least partially through the AMPK pathway.

Collectively, we show that hypoxia-induced constant EglN1-AMPKα interaction leads to their accumulation on mitochondria, EglN1 recruits CaMKK2 to AMPKα, thus resulting in the formation of CaMKK2-EglN1-AMPKα complex for AMPKα phosphorylation, thereby ensuring metabolic homeostasis and breast tumor growth (Fig 6H).

Discussion

Mitochondria are the largest consumers of intracellular oxygen, and their metabolic adaptation to hypoxia plays an essential role in tumor malignancy and therapy resistance (Valcarcel-Jimenez *et al*, 2017; Bargiela *et al*, 2018). However, the mechanism of how mitochondria respond to hypoxia remains elusive. Here, we find that hypoxia induces translocation of EglN1 to mitochondria. EglN1 β2β3 loop region is required for its mitochondrial translocation and breast tumor growth. Further, we reveal compartmentalized oxygen sensing pathway EglN1-VHL-AMPKα on mitochondria under normoxia. Specifically, EglN1 catalyzes prolyl-hydroxylation of

Figure 6. EglN1 recruiting CaMKK2 to AMPKα under hypoxia is essential for breast tumor growth.

A Immunoblots of mitochondrial extracts (Mito) and immunoprecipitations (IP) generated in (Fig 4F).

B Immunoblots (IB) of whole cell extracts (WCE) and immunoprecipitations (IP) of T47D cells infected with control shRNA (−) or EglN1 sh1045 (EglN1 shRNA) with or without hypoxia treatment (1% O_2 for 24 h).

C, D Immunoblots (C) and MTT assays (D) of T47D (left panel) and MDA-MB-231 (right panel) cells infected with control vector (Ctrl) or AMPKα-T172D-Flag followed by infection with control shRNA (shCtrl) or EglN1 sh1045 (EglN1 shRNA) under hypoxic (1% O_2) condition.

E–G Mouse xenograft experiments were performed with the MDA-MD-MB231 cells generated in (C). Tumor growth curves (E) and tumor weights (F) were calculated, and gross tumors (G) were presented (n = 6 mice per group).

H A proposed model depicting the regulatory mechanism of mitochondrial EglN1 under hypoxia.

Data information: Error bars in (D–F) represent ± SEM, *** denotes P value of 0.005 (unpaired t-test). n = 3 independent technical replicate experiments for MTT assays. Also See Fig EV5.
Source data are available online for this figure.

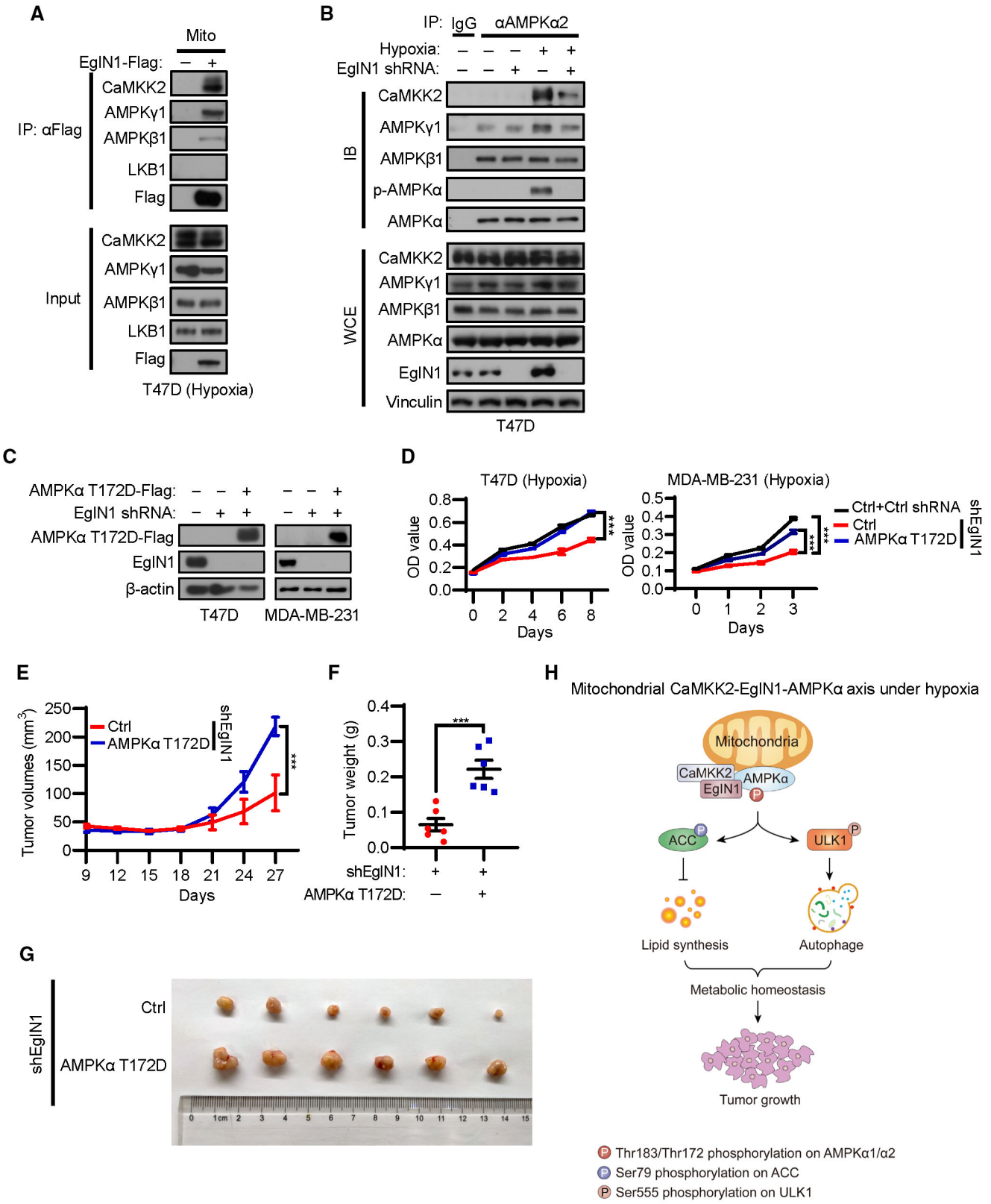

Figure 6.

AMPKα, and VHL targets hydroxylated-AMPKα for dephosphorylation under normoxia (Fig 4U). While hypoxia induces the formation of CaMKK2-EglN1-AMPKα complex on mitochondria where AMPKα is activated to ensure metabolic homeostasis and tumor cell growth (Fig 6I). Thus, our findings underline the significance of EglN1 as an oxygen sensor that functions not only under normoxia but also hypoxia.

The mitochondrial translocation of EglN1 under hypoxia is in a time-dependent manner, and reoxygenation after hypoxia treatment can lead to EglN1 release from mitochondria. This dynamic and reversible process may reflect mitochondrial sensing of hypoxic stress, although the effects of reoxygenation are slow, which might be due to some component(s) secreted into the culture media from hypoxic cells that could transmit the leftover hypoxic stress and prolong the effect of hypoxia on EglN1. The underlying mechanism requires future study. Moreover, we have identified EglN1 β2β3 loop responsible for its mitochondrial translocation upon hypoxia, but the EglN1 loss of β2β3 loop mutant still showed localization on mitochondria, we speculate that other region(s) of EglN1 may also contribute to its mitochondrial localization, but the event for hypoxia-induced mitochondrial translocation of EglN1 requires the β2β3 loop.

VHL targets prolyl-hydroxylated proteins for proteasomal degradation or protein dephosphorylation, e.g., VHL targets hydroxylated-HIFα for ubiquitylation and degradation (Berra *et al*, 2003; Kaelin & Ratcliffe, 2008), and it also recognizes hydroxylated-Akt for dephosphorylation (Guo *et al*, 2016). Similar to VHL regulation of Akt, we found that AMPKα is prolyl-hydroxylated by EglN1 and subsequently targeted by VHL for dephosphorylation under normoxia.

Hypoxia drives tumor aggressiveness, metabolic adaptation to hypoxic stress plays an essential role during these processes, where mitochondria are the central hub (Lee *et al*, 2020b). The outer mitochondrial membrane serves as a major signaling platform to regulate cell signaling (Tan & Finkel, 2020; Picard & Shirihai, 2022). Our findings reveal a regulatory mechanism for EglN1 in breast cancer, in which EglN1 is a key oxygen-sensitive metabolic checkpoint enabling the outer mitochondrial membrane to sense hypoxic signal. The prolyl hydroxylases EglN family (EglN1/2/3) are well-studied oxygen sensors with remarkably high sensitivity to fluctuations in oxygen in various tissues (Losman *et al*, 2020), among those, EglN1 is established as the most important oxygen sensor (Schofield & Ratcliffe, 2004; Takeda *et al*, 2006). EglN1 hydroxylates HIFα occurred in the nucleus (Groulx & Lee, 2002; Wotzlaw *et al*, 2010; Pientka *et al*, 2012), and previous studies have been focused on the regulatory mechanisms of EglN1 under normoxia with its intact enzymatic activity. But, EglN1 is mainly located in the cytoplasm (Metzen *et al*, 2003), and its related signaling in the cytoplasmic compartments, and in stress conditions such as hypoxia, has been generally overlooked. In this study, we identify a compartmentalized oxygen sensing signaling EglN1-AMPKα axis on the outer mitochondrial membrane, hypoxia induces constant EglN1-AMPKα interaction through EglN1 substrate binding region β2β3 loop, leading to their accumulation on mitochondria and activation of the AMPK pathway.

HIF is a well-established transcription factor to reduce mitochondrial activity through transcriptional activation of its target genes, such as COX4I2, LON, LDHA and PDK1 which are involved in modulation of ETC activity and the TCA cycle (Iyer *et al*, 1998; Kim *et al*, 2006; Papandreou *et al*, 2006; Lee *et al*, 2020b). Several studies have also revealed the localization of HIF with mitochondria under oxidative stress (Rane *et al*, 2009; Briston *et al*, 2011; Li *et al*, 2019). Here, the mitochondrial proteomics data showed that HIF was not localized to mitochondria in T47D breast cancer cells. Also, through mitochondrial extraction followed by Western blotting assays, we found that HIF is barely detectable in the mitochondria of breast cancer cells, suggesting that the mitochondrial localization of HIF is cell context-dependent. Inhibition of HIF by the inhibitor PT2399 had no effect on EglN1 mitochondrial translocation and its regulation of breast cancer cell growth, underlying the important role of mitochondrial EglN1 that is independent of the HIF pathway.

It has reported that the interactions between EglN and its substrates rapidly dissociates following hydroxylation, while hypoxia can trap their enzyme-substrate interactions (Zurlo *et al*, 2019). However, it remains unknown whether the hypoxia-induced enzyme-substrate interactions could be a hypoxic signal and functionally important. Here, we show a previously unrecognized role of mitochondrial EglN1 in hypoxia signaling through enzyme-substrate interactions, thus underlining the important role of EglN1 as an oxygen sensor that functions not only under normoxia but also hypoxia.

AMPK is a master regulator for restoring metabolic homeostasis during various metabolic stresses, it is a well-known energy sensor required for tumor cell survival under metabolic stresses (Wang *et al*, 2016; Garcia & Shaw, 2017; Lee *et al*, 2020a,b; Trefts & Shaw, 2021). Also, AMPKα phosphorylation under hypoxic stress is crucial for restoring metabolic homeostasis to allow continued cell proliferation (Emerling *et al*, 2009), but the underlying mechanism is not fully understood. Previous studies have reported that hypoxia induces mitochondrial calcium release, which can activate CaMKK2, leading to AMPKα phosphorylation activation (Waypa *et al*, 2002; Gusarova *et al*, 2011; Mungai *et al*, 2011). Here, we found that EglN1 interacted with both AMPKα and CaMKK2 on mitochondria during hypoxia. Depletion of EglN1 inhibited the hypoxia-induced interaction between AMPKα and CaMKK2, and in the meantime decreased the phosphorylation levels of AMPKα. Therefore, we conclude that EglN1 serves as a scaffold protein linking CaMKK2 to AMPKα for AMPKα phosphorylation activation. However, some critical questions about whether EglN1 participates in hypoxia-induced CaMKK2 activation and how EglN1 regulates CaMKK2 activity require future investigation. In summary, we identify AMPKα as a substrate of EglN1, the substrate binding region β2β3 loop of EglN1 linked to AMPKα enables the immediate response of the AMPK pathway to oxygen changes, loss of EglN1 β2β3 loop interrupts this process. Our data suggest that EglN1 β2β3 loop is a promising therapeutic target for breast cancer.

Materials and Methods

Cell culture and reagents

MDA-MB-231 (ATCC HTB-26), 786-O (ATCC CRL-1932), and 293T (ATCC CRL-3216) were cultured in DMEM (C11995500BT) containing 10% fetal bovine serum plus 1% penicillin–streptomycin. T47D (ATCC HTB-133) was maintained in RPMI (C11875500BT) medium supplemented with 10% fetal bovine serum and 1%

penicillin–streptomycin. All cells were maintained at 37°C in 5% CO_2 incubator. Dimethyloxaloylglycine (DMOG, S7483), and Compound C (AMPK inhibitor, S7840) were from Selleck. Deferoxamine (DFO, HY-B0988), 2,3-Dimethoxy-1,4-naphthoquinone (DMNQ, HY-121026), and PT2399 (HY-108697) were from MedChemExpress. The above reagents were used at the indicated doses as previously described (Liu *et al*, 2011; Zhang *et al*, 2015; Guo *et al*, 2016; Ciotti *et al*, 2020; Dai *et al*, 2021). Hypoxia treatment was performed with hypoxia workstation (Baker Ruskinn's $InvivO_2$ 400).

Western blot analysis and antibodies

EBC buffer (50 mM Tris pH8.0, 120 mM NaCl, 0.5% NP40, 0.1 mM EDTA and 10% Glycerol) supplemented with complete protease inhibitor (Roche Applied Biosciences) was used to harvest whole cell lysates. Subcellular protein Fractionation kit was obtained from Beyotime Biotechnology. Cell lysate concentrations were measured by Thermo Scientific BCA kit (23227). Equal amounts of cell lysates were resolved by SDS–PAGE. The experiments were repeated for three times with similar results. Rabbit antibody anti-EglN1 (4835S), anti-HIF1α (36169S), anti-HIF1β (5537S), anti-HIF2α (59973S), anti-AMPKα (2532S, for WB), anti-Phospho-AMPKα (T172, 2535T), anti-Acetyl-CoA Carboxylase (ACC, 3662S), anti-Phospho-ACC Ser79 (p-ACC Ser79, 11818S), anti-ULKI (8054T), anti-Phospho-ULK1 Ser555 (5869T), anti-AMPKγ1 (4187T), anti-AMPKα1 (2795S, for WB), anti-AMPKα2 (2757T, for WB), LC3B (3868S), anti-His (12698) and anti-hemagglutinin (HA, 3724S, for WB) were from Cell Signaling Technology. Mouse antibody anti-αTubulin (3873S) and AMPKα (2793S, for IP) were obtained from Cell Signaling Technology. Rabbit antibody anti-H3 (17168-1-AP), anti-Flag (20543-1-AP, for WB), anti-VHL (24756-1-AP), anti-SDHA (14865-1-AP), anti-AIF (17984-1-AP), anti-LKB1 (10746-1-AP), anti-CaMKK2 (11549-1-AP), anti-PP2CA (13482-1-AP), AMPKβ1 (10308-1-AP), anti-Flag (20543-1-AP) and anti-TOMM20 (11802-1-AP) were from Proteintech. Rabbit antibody AMPKα1 (ab32047, for IP) and AMPKα2 (ab214425, for IP) were from abcam. Mouse antibody β-actin (A5441), Vinculin (V9131), and anti-Flag (F3165) were from Sigma. Mouse antibody HA-tag (901514, for IP) was from Biolegend. Peroxidase conjugated goat anti-mouse secondary antibody (170-6516) and peroxidase conjugated goat anti-rabbit secondary antibody (170-6515) were purchased from BIO-RAD. Hydroxyl-AMPKα1/2-Pro188/177 antibodies were generated by Mabnus Biological Technology Incorporation.

Plasmids

Full-length FLAG tagged EglN1 were amplified by PCR with a FLAG tag with a 5′ primer that introduced a MluI site and a 3′ primer that introduced a BamHI site. The PCR products were digested with the corresponding enzymes and cloned into the pHAGE-puromycin vector. pcDNA-3.1-HA-VHL, pHAGE-AMPKα1/α2/P188A/P177A-flag, pHAGE-EglN1-P317R-flag, pMSCV-EglN1-WT/P317R-flag, pMSCV-TOM20-EglN1-WT/P317R-flag, pMSCV-TOM20-EglN1-WT/P317R-flag (EglN1 sh1045-resistant) were constructed using standard molecular biology techniques. Mut Express II Fast Mutagenesis Kit V2 (C214-01, Vazyme) was used to construct EglN1 and AMPKα1/2 mutants. All plasmids were sequenced for validation. Lentiviral shRNA and sgRNA target sequences were used as previous described (Zhang *et al*, 2018):

Control shRNA: AACAGTCGCGTTTGCGACTGG
EglN1 shRNA (1042): CTGTTATCTAGCTGAGTTCAT
EglN1 shRNA (1045): TGGAGATGGAAGATGTGTGAC
HIF1β shRNA (1770): GAGAAGTCAGATGGTTTATTT
HIF1α shRNA (3809): CCAGTTATGATTGTGAAGTTA
HIF2α shRNA (3804): CGACCTGAAGATTGAAGTGAT
AMPKα1 shRNA (690): GAAGGTTGTAAACCCATATTA
AMPKα1 shRNA (860): TGATTGATGATGAAGCCTTAA
AMPKα1 shRNA (831): GTGACCTCACTTGACTCTTCT
AMPKα2 shRNA (171): CCCACTGAAACGAGCAACTAT
AMPKα2 shRNA (523): GTCATCCTCATATTATCAAAC
Control sgRNA: GCGAGGTATTCGGCTCCGCG
VHL sgRNA: ACCGAGCGCAGCACGGGCCG

Transfection

Cells (approximately 50% confluency) were seeded on indicated dishes. Cells were transfected the following day with Lipofectamine 3000 transfection reagent (L3000015, Thermo Fisher Scientific) and harvested 48 h after transfection.

Virus production and infection

293T packaging cell lines were used for lentiviral/retroviral amplification. Lentiviral/retroviral infection was performed as previously described (Zhang *et al*, 2018). Briefly, cells were transfected with lipofectamine 3000, viruses were collected twice after 48 and 72 h. After passing through 0.45 μM filters, appropriate amount of viruses was used to infect target cells in the presence of 8 μg/ml polybrene. Subsequently on the next day, the target cell lines underwent appropriate antibiotic selection.

Cell proliferation assays

Cells were seeded in triplicate onto 96-well plates (1,500 cells/well) in appropriate growth medium. At indicated time points, cells were replaced with 90 μl fresh growth medium supplemented with 10 μl 0.5 μg/ml 3-(4,5-dimethyl-2-thiazolyl)-2,5-diphenyl-2-H-tetrazolium bromide (BioFrox, 143315), followed by incubation at 37°C for 2 h. Then, this medium was removed completely, and 100 μl DMSO was added to well. Finally, the cell growth was measured by Microplate Reader at 490 nm wavelength.

Colony formation assays

Cells were seeded into 12-well plates (1,500 cells/well for MDA-MB-231 or 5,000 cells/well for T47D) and left for 8–12 days until formation of visible colonies. Colonies were washed with PBS and fixed with 4% paraformaldehyde for 20 min, then stained with 0.8% crystal violet for 20 min. After staining, the plates were washed and air-dried. Three independent experiments were performed to generate the consistent result.

Mitochondria isolation and proteinase K treatment

Mitochondria were extracted with Cell Mitochondria Isolation Kit (Beyotime Biotechnology, C3601) according to the manufacturers' protocol. In brief, harvested cells were washed twice with cold PBS

and disrupted mechanically with a Dounce homogenizer in cell mitochondria isolation reagent plus PMSF, and then incubated on ice for 15 min. The cell solutions were centrifuged at 1,000 *g* for 10 min at 4°C, and the cell debris and nuclei were removed to obtain the supernatant. Mitochondrial fractions were pelleted by centrifugation at 12,000 *g* for 20 min. The final supernatant was subjected to 16,000 *g* centrifugation for 20 min at 4°C to isolate cytosol. For Proteinase K assay, the freshly isolated mitochondria were incubated with the indicated concentrations of Proteinase K (Millipore, 3016611) for 30 min on ice, the reaction was terminated by PMSF (1 mM) and analyzed by immunoblot analysis (Yan *et al*, 2020).

Immunoprecipitation

Cells were lysed in EBC lysis buffer supplemented with complete protease inhibitors (Roche Applied Bioscience). Lysates were clarified by centrifugation at 16,000 *g* for 20 min, and then mixed with primary antibodies or Flag-conjugated beads (Sigma, A2220) overnight. For primary antibody incubation overnight, cell lysates were further incubated with protein G sepharose beads (Thermo Fisher Scientific, 20399) for 2 h. Bound complexes were washed with NETN buffer six times and were eluted by boiling in SDS loading buffer. Bound proteins were resolved in SDS–PAGE followed by Western blot analysis (Zhang *et al*, 2015).

Immunofluorescence

Cells expressing EglN1-GFP were cultured on coverslips in 24-well plates, and were exposed to normoxia or hypoxia for 24 h at 37°C incubator. Cells were washed once with PBS after MitoTracker staining for 30 min at 37°C incubator and were fixed with 4% paraformaldehyde for 20 min at room temperature. The nucleus was stained with 4,6-diamidino-2-phenylindole (DAPI). Zeiss LSM880 with Airyscan confocal microscopy was used to take images. Quantification of the co-localization was determined by ImageJ software.

Six patient breast tumor samples were obtained from Zhongnan Hospital of Wuhan university and approved by the Medical Ethics Committees of School of Medicine, Wuhan University. A human breast cancer tissue microarray was obtained from Outdo Biotech (Shanghai, China, permit number is HBreD080CS01). Tumor samples were formalin-fixed, paraffin-embedded, and sectioned according to the standard protocol (Meng *et al*, 2022). After antigen retrieval in citrate buffer at 95°C, samples were blocked in 5% BSA with 0.1% Triton X-100 for 1 h at room temperature, and then incubated sequentially with primary antibodies against TOM20 (Proteintech, 66777-1-Ig, 1:100) and EglN1 (PA5-78511, Thermo Fisher, 1:100) or HIF (sc-13515, 1:100) at 4°C overnight, followed by their respective secondary fluorescently labeled antibodies (Invitrogen, 1:250) for 40 min at room temperature. Images were obtained by using Leica confocal microscopy or Zeiss LSM880 confocal microscopy. Immunofluorescence mean fluorescence intensity statistics using FIJI (v1.53t) (https://doi.org/10.1038/nmeth.2019). Threshold was used with the default segmentation mode. Co-localization analysis was used with the Colocalization finder plugin (v1.6) in FIJI. Samples without tumor cells were removed from the analysis. Statistical analysis was performed with GraphPad Prism 8 (v8.0.2). Correlation between co-localization of EglN1 with TOM20 and the intensity of HIF1α was evaluated by Pearson Correlation Test. Values were considered significant if $P < 0.05$.

GST fusion protein purification and pull-down assays

pGEX-4T-1 construct was transformed into BL21-competent cells. Starter cultures (5 ml) overnight at 37°C were inoculated (1%) into larger volumes (500 ml) with ampicillin, respectively. The bacteria were grown at 37°C until an OD600 of 0.8–1.0, following which protein expression was induced for 12–16 h using 0.2 mM IPTG at 16°C with vigorous shaking. Bacterial pellets were harvested by centrifugation and sonicated by a Nano DeBEE homogenizer. Cleared bacterial lysates were purified using Glutathione-sepharose 4B (GE healthcare, 17-0755-01). GST-bound proteins (20 μl) were incubated with *in vitro* translated protein. After 4 h incubation, bound complexes were washed four times with NETN buffer, followed by boiling in SDS loading buffer and solving in SDS–PAGE.

Peptide synthesis

N-terminal biotinylated peptides used for pull-down assays were synthesized by Mabnus Biological Technology Incorporation. The sequences were listed below:

AMPKα1/2-Pro188/177-WT (aa182-203/171–192): RTSCGSPNYAAP EVISGRLYAG
AMPKα1/2-Pro188/177-OH (aa182-203/177–192): RTSCGS**P***(OH) NYAAPEVISGRLYAG

Peptides were diluted into 2 μg/μl for further biochemical assays.

Dot immunoblot assays

A volume of 1 μl peptides were spotted onto nitrocellulose membrane. The membrane was dried and blocked in non-specific sites by soaking in TBST buffer with 5% non-fat milk for immunoblot analysis (Guo *et al*, 2016).

Peptide-binding assays

Peptides (2 μg) were incubated with 1 mg of 500 μl cell lysates for 10 h at 4°C and then added 15 μl Streptavidin agarose (MedChemExpress, HY-K0218) for another 2 h. The agarose was washed four times with NETN buffer. Bound proteins were eluted by boiling in SDS loading buffer and resolved by SDS–PAGE and then followed by immunoblot analysis (Guo *et al*, 2016).

In vitro hydroxylation assays

Purification of GST-EglN1 WT and its P317R mutant recombinant protein were performed as described above. The vitro hydroxylation assays was performed as previously reported (Li *et al*, 2022). Briefly, 10 μg AMPKα-biotinylated peptides were added to 60 μl of hydroxylation reaction buffer supplemented with 100 μM $FeCl_2$, 2 mM ascorbate, and 5 mM 2-oxoglutarate. recombinant protein GST-EglN1 WT or mutant (2 μg) was added to start the

hydroxylation reaction. After incubation for 2 h at 37°C, the reactions were subjected to immunoblot analysis.

Tandem mass tag (TMT) quantitative analyses of mitochondrial proteomes

To profile mitochondrial proteomes under normoxia and hypoxia, mitochondria were isolated by Cell Mitochondria Isolation Kit (Beyotime Biotechnology, C3601) according to the manufacturers' protocol from T47D cells with normoxia or hypoxia treatment for 24 h, which was performed in triplicates. Then, Applied Protein Technology performed quantitative mitochondrial proteomics by TMT labeling. Briefly, SDT buffer (4%SDS, 100 Mm Tris/HCl Ph7.6, 0.1 M DTT) was used for mitochondria lysis, mitochondria extraction is then digested by filter-aided sample preparation (FASP). 100 μg peptide mixture of each sample was labeled by Tandem Mass Tag (TMT). Subsequently, the resulting peptides went through fractionation and were analyzed by LC–MS/MS. Data were analyzed by Proteome Discoverer (v.1.4, Thermo Scientific) against the human UniProt Reference Proteome database.

Bioinformatics analyses of mitochondrial proteomes

The proteomics profiling was analyzed and visualized using R statistical software version 4.2.0. Differentially expressed proteins were identified by using the unpaired two-tail student's *t*-test with the thresholds of ± 1.2-fold change (FC) over the normoxia group (i.e., hypoxia/normoxia ratio > 1.2 or < 0.83) and an adjusted *P*-value < 0.05.

GSEA based on GO was performed through the 'gseGO' function in clusterProfiler package (v4.4.1) (https://doi.org/10.1016/j.xinn.2021.100141). A ranked gene list of all proteins was generated according to the value of log2FC. GO includes three categories: molecular function (MF), biological process (BP), and cellular component (CC). We selected 'BP' in the present study to perform the GO analysis. The adjusted *P*-value < 0.05 was set as the cut-off criteria. The connections between the significantly enriched oxygen-related GO terms and participating proteins were visualized by Cytoscape (v3.9.1) (https://doi.org/10.1101%2Fgr.1239303) with a network diagram.

PLS-DA was conducted by the 'plsda' function of mixOmics package (v6.20.0). The heatmaps were drawn with the pheatmap packages (v1.0.12) and other plots were generated using ggplot2 packages (v3.3.6).

Immunoprecipitation and mass spectrometry (IP-MS)

To determine the EglN1-interacting proteins, EglN1-Flag and its bound proteins were immunoprecipitated with Flag-beads from T47D cells (1×10^8) stably expressing EglN1-Flag followed by LC–MS/MS, and the data were analyzed using Proteome Discoverer (v.2.2, Thermo Scientific).

Identification of prolyl-hydroxylation sites by mass spectrometry

To identify prolyl-hydroxylated sites on AMPKα1 and AMPKα2, 786O cells were infected with lentivirus expressing AMPKα1-Flag or AMPKα2-Flag, and subsequently treated with DMSO or DMOG (2 mM) for 24 h. Cells were lysed in EBC buffer supplemented with protease inhibitor and phosphatase inhibitor. Cell lysates were then incubated with FLAG-beads (Sigma, A2220) at 4°C overnight to pull down AMPKα1-Flag or AMPKα2-Flag. Beads were washed four times by NETN buffer and the bound proteins were resolved by SDS–PAGE. The gels were stained by Commassie Brilliant Blue (C8420, Solarbio) and AMPKα1-Flag and AMPKα2-Flag bands were excised, respectively, for LC–MS/MS analysis as previously described (Zhang *et al*, 2018).

Mouse orthotopic tumor growth

Six-week old female nude mice were obtained from GemPharmatech and used for our xenograft studies ($n = 6$/group). Approximately 1×10^6 viable cells of each group were orthotopically injected into the mammary gland as described previously (Zhang *et al*, 2009). Tumor size was measured every three days with a caliper, and the tumor volume was determined with the formula: $L \times W^2 \times 0.5$ (L is the longest diameter and W is the shortest diameter). After 27 days, all mice were sacrificed and those solid tumors were dissected, tumor weights were measured and recorded post-necropsy. Mice were bred and maintained in Animal Center of Medical Research Institute at Wuhan University. All animal experiments were performed according to protocols approved by the Animal Care and Use Committee of Medical Research Institute, Wuhan University.

Statistical analysis

The unpaired two-tail student's *t*-test was used for experiments comparing two sets of data. Data represent mean ± SEM from three independent experiments. *, ** and *** denotes *P* value of < 0.05, 0.01 and 0.005 respectively. NS denotes not significance.

Data availability

The LC–MS/MS data for mitochondrial proteomics have been deposited to the ProteomeXchange Consortium with the dataset identifier PXD041653.

Expanded View for this article is available online.

Acknowledgements

The authors thank members of our laboratory for helpful discussions. We thank Dr. Hong-Bing Shu (Wuhan University) and Dr. Chen-Song Zhang (Xiamen University) for providing critical plasmids. This work is supported by the Fundamental Research Funds for the Central Universities 2042020kf0197 (JZ), National Natural Science Foundation of China 31970737 (JZ) and 32100570 (CY), the Startup Funding from Wuhan University (JZ), Natural Science Foundation of Hubei Province 2020CFA071 (JZ), the Natural Science Foundation of Hubei Province of China 2022CFA008 (JZ), the Fundamental Research Funds for the Central Universities 2042022dx0003 (JZ), the National Key Research and Development Program of China 2022YFA1305400 (JZ), Research Project established by Chinese Pharmaceutical Association Hospital Pharmacy Department CPA-Z05-ZC-2022-002 (HH) and the China Postdoctoral Science Foundation 2020M672408 (CY). We also sincerely thank the core facility of the Medical Research Institute at Wuhan University for their technical support.

Author contributions

Jing Zhang: Conceptualization; resources; data curation; formal analysis; supervision; funding acquisition; validation; investigation; visualization; methodology; writing – original draft; project administration; writing – review and editing. **Weiwei Jiang:** Data curation; formal analysis; validation; investigation; visualization; methodology; writing – original draft; writing – review and editing. **Mengyao Zhang:** Data curation; formal analysis; validation; investigation; visualization. **Chuan Gao:** Data curation; formal analysis; visualization; methodology. **Chaojun Yan:** Data curation; formal analysis; funding acquisition; investigation; visualization; methodology. **Ziwei He:** Data curation; investigation. **Xin Wei:** Formal analysis; visualization; methodology. **Jingjing Xiong:** Validation; investigation. **Zilun Ruan:** Formal analysis; investigation; visualization. **Jinpeng Li:** Resources; investigation. **Qifang Li:** Formal analysis; validation; investigation. **Ziyi Zhong:** Investigation. **Mengna Zhang:** Resources. **Qianqian Yuan:** Investigation. **Shuang Wang:** Validation; methodology. **Ming-Ming Hu:** Resources. **Cheguo Cai:** Resources. **Gao-Song Wu:** Resources. **Chao Jiang:** Resources; formal analysis. **Ya-Lin Zhang:** Resources; investigation. **Chen-Song Zhang:** Resources; investigation; methodology; writing – review and editing. **Ronghui Gao:** Data curation; formal analysis; investigation; methodology. **Qian Yang:** Investigation. **Hankun Hu:** Resources; funding acquisition.

Disclosure and competing interests statement

The authors declare that they have no conflict of interest.

References

Bargiela D, Burr SP, Chinnery PF (2018) Mitochondria and hypoxia: metabolic crosstalk in cell-fate decisions. *Trends Endocrinol Metab* 29: 249 – 259

Batie M, Frost J, Frost M, Wilson JW, Schofield P, Rocha S (2019) Hypoxia induces rapid changes to histone methylation and reprograms chromatin. *Science* 363: 1222 – 1226

Bell EL, Chandel NS (2007) Mitochondrial oxygen sensing: regulation of hypoxia-inducible factor by mitochondrial generated reactive oxygen species. *Essays Biochem* 43: 17 – 27

Berra E, Benizri E, Ginouves A, Volmat V, Roux D, Pouyssegur J (2003) HIF prolyl-hydroxylase 2 is the key oxygen sensor setting low steady-state levels of HIF-1alpha in normoxia. *EMBO J* 22: 4082 – 4090

Bhandari V, Hoey C, Liu LY, Lalonde E, Ray J, Livingstone J, Lesurf R, Shiah YJ, Vujcic T, Huang X *et al* (2019) Molecular landmarks of tumor hypoxia across cancer types. *Nat Genet* 51: 308 – 318

Briggs KJ, Koivunen P, Cao S, Backus KM, Olenchock BA, Patel H, Zhang Q, Signoretti S, Gerfen GJ, Richardson AL *et al* (2016) Paracrine induction of HIF by glutamate in breast cancer: EglN1 senses cysteine. *Cell* 166: 126 – 139

Briston T, Yang J, Ashcroft M (2011) HIF-1alpha localization with mitochondria: a new role for an old favorite? *Cell Cycle* 10: 4170 – 4171

Buffa FM, Harris AL, West CM, Miller CJ (2010) Large meta-analysis of multiple cancers reveals a common, compact and highly prognostic hypoxia metagene. *Br J Cancer* 102: 428 – 435

Chakraborty AA, Laukka T, Myllykoski M, Ringel AE, Booker MA, Tolstorukov MY, Meng YJ, Meier SR, Jennings RB, Creech AL *et al* (2019) Histone demethylase KDM6A directly senses oxygen to control chromatin and cell fate. *Science* 363: 1217 – 1222

Chowdhury R, McDonough MA, Mecinovic J, Loenarz C, Flashman E, Hewitson KS, Domene C, Schofield CJ (2009) Structural basis for binding of hypoxia-inducible factor to the oxygen-sensing prolyl hydroxylases. *Structure* 17: 981 – 989

Ciotti S, Iuliano L, Cefalu S, Comelli M, Mavelli I, Di Giorgio E, Brancolini C (2020) GSK3 beta is a key regulator of the ROS-dependent necrotic death induced by the quinone DMNQ. *Cell Death Dis* 11: 2

Curtis C, Shah SP, Chin SF, Turashvili G, Rueda OM, Dunning MJ, Speed D, Lynch AG, Samarajiwa S, Yuan Y *et al* (2012) The genomic and transcriptomic architecture of 2,000 breast tumours reveals novel subgroups. *Nature* 486: 346 – 352

Dai XM, Bu X, Gao Y, Guo JP, Hu J, Jiang C, Zhang Z, Xu KX, Duan JZ, He SH *et al* (2021) Energy status dictates PD-L1 protein abundance and anti-tumor to enable blockade. *Mol Cell* 81: 2317 – 2331

Elvidge GP, Glenny L, Appelhoff RJ, Ratcliffe PJ, Ragoussis J, Gleadle JM (2006) Concordant regulation of gene expression by hypoxia and 2-oxoglutarate-dependent dioxygenase inhibition: the role of HIF-1alpha, HIF-2alpha, and other pathways. *J Biol Chem* 281: 15215 – 15226

Emerling BM, Weinberg F, Snyder C, Burgess Z, Mutlu GM, Viollet B, Budinger GR, Chandel NS (2009) Hypoxic activation of AMPK is dependent on mitochondrial ROS but independent of an increase in AMP/ATP ratio. *Free Radic Biol Med* 46: 1386 – 1391

Flashman E, Bagg EA, Chowdhury R, Mecinovic J, Loenarz C, McDonough MA, Hewitson KS, Schofield CJ (2008) Kinetic rationale for selectivity toward N- and C-terminal oxygen-dependent degradation domain substrates mediated by a loop region of hypoxia-inducible factor prolyl hydroxylases. *J Biol Chem* 283: 3808 – 3815

Garcia D, Shaw RJ (2017) AMPK: mechanisms of cellular energy sensing and restoration of metabolic balance. *Mol Cell* 66: 789 – 800

Gerald D, Berra E, Frapart YM, Chan DA, Giaccia AJ, Mansuy D, Pouyssegur J, Yaniv M, Mechta-Grigoriou F (2004) JunD reduces tumor angiogenesis by protecting cells from oxidative stress. *Cell* 118: 781 – 794

Groulx I, Lee S (2002) Oxygen-dependent ubiquitination and degradation of hypoxia-inducible factor requires nuclear-cytoplasmic trafficking of the von Hippel-Lindau tumor suppressor protein. *Mol Cell Biol* 22: 5319 – 5336

Guo J, Chakraborty AA, Liu P, Gan W, Zheng X, Inuzuka H, Wang B, Zhang J, Zhang L, Yuan M *et al* (2016) pVHL suppresses kinase activity of Akt in a proline-hydroxylation-dependent manner. *Science* 353: 929 – 932

Gusarova GA, Trejo HE, Dada LA, Briva A, Welch LC, Hamanaka RB, Mutlu GM, Chandel NS, Prakriya M, Sznajder JI (2011) Hypoxia leads to Na,K-ATPase downregulation via Ca(2+) release-activated Ca(2+) channels and AMPK activation. *Mol Cell Biol* 31: 3546 – 3556

Hu L, Xie H, Liu X, Potjewyd F, James LI, Wilkerson EM, Herring LE, Xie L, Chen X, Cabrera JC *et al* (2020) TBK1 Is a synthetic lethal target in cancer with VHL loss. *Cancer Discov* 10: 460 – 475

Iyer NV, Kotch LE, Agani F, Leung SW, Laughner E, Wenger RH, Gassmann M, Gearhart JD, Lawler AM, Yu AY *et al* (1998) Cellular and developmental control of O_2 homeostasis by hypoxia-inducible factor 1 alpha. *Genes Dev* 12: 149 – 162

Kaelin WG Jr, Ratcliffe PJ (2008) Oxygen sensing by metazoans: the central role of the HIF hydroxylase pathway. *Mol Cell* 30: 393 – 402

Kim JW, Tchernyshyov I, Semenza GL, Dang CV (2006) HIF-1-mediated expression of pyruvate dehydrogenase kinase: a metabolic switch required for cellular adaptation to hypoxia. *Cell Metab* 3: 177 – 185

Kohl R, Zhou J, Brune B (2006) Reactive oxygen species attenuate nitric-oxide-mediated hypoxia-inducible factor-1alpha stabilization. *Free Radic Biol Med* 40: 1430 – 1442

Lando D, Peet DJ, Gorman JJ, Whelan DA, Whitelaw ML, Bruick RK (2002) FIH-1 is an asparaginyl hydroxylase enzyme that regulates the transcriptional activity of hypoxia-inducible factor. *Genes Dev* 16: 1466 – 1471

Lee KH, Choi E, Chun YS, Kim MS, Park JW (2006) Differential responses of two degradation domains of HIF-1alpha to hypoxia and iron deficiency. *Biochimie* 88: 163 – 169

Lee DC, Sohn HA, Park ZY, Oh S, Kang YK, Lee KM, Kang M, Jang YJ, Yang SJ, Hong YK *et al* (2015) A lactate-induced response to hypoxia. *Cell* 161: 595 – 609

Lee G, Won HS, Lee YM, Choi JW, Oh TI, Jang JH, Choi DK, Lim BO, Kim YJ, Park JW *et al* (2016) Oxidative dimerization of PHD2 is responsible for its inactivation and contributes to metabolic reprogramming via HIF-1alpha activation. *Sci Rep* 6: 18928

Lee H, Zandkarimi F, Zhang Y, Meena JK, Kim J, Zhuang L, Tyagi S, Ma L, Westbrook TF, Steinberg GR *et al* (2020a) Energy-stress-mediated AMPK activation inhibits ferroptosis. *Nat Cell Biol* 22: 225 – 234

Lee P, Chandel NS, Simon MC (2020b) Cellular adaptation to hypoxia through hypoxia inducible factors and beyond. *Nat Rev Mol Cell Biol* 21: 268 – 283

Li HS, Zhou YN, Li L, Li SF, Long D, Chen XL, Zhang JB, Feng L, Li YP (2019) HIF-1alpha protects against oxidative stress by directly targeting mitochondria. *Redox Biol* 25: 101109

Li S, Li W, Yuan J, Bullova P, Wu J, Zhang X, Liu Y, Plescher M, Rodriguez J, Bedoya-Reina OC *et al* (2022) Impaired oxygen-sensitive regulation of mitochondrial biogenesis within the von Hippel-Lindau syndrome. *Nat Metab* 4: 739 – 758

Liu JL, Mao ZY, Gallick GE, Yung WKA (2011) AMPK/TSC2/mTOR-signaling intermediates are not necessary for LKB1-mediated nuclear retention of PTEN tumor suppressor. *Neuro Oncol* 13: 184 – 194

Liu X, Simon JM, Xie H, Hu L, Wang J, Zurlo G, Fan C, Ptacek TS, Herring L, Tan X *et al* (2020) Genome-wide screening identifies SFMBT1 as an oncogenic driver in cancer with VHL loss. *Mol Cell* 77: 1294 – 1306

Liu X, Wang J, Boyer JA, Gong W, Zhao S, Xie L, Wu Q, Zhang C, Jain K, Guo Y *et al* (2022) Histone H3 proline 16 hydroxylation regulates mammalian gene expression. *Nat Genet* 54: 1721 – 1735

Losman JA, Koivunen P, Kaelin WG Jr (2020) 2-Oxoglutarate-dependent dioxygenases in cancer. *Nat Rev Cancer* 20: 710 – 726

Meng Y, Qiu L, Zeng X, Hu X, Zhang Y, Wan X, Mao X, Wu J, Xu Y, Xiong Q *et al* (2022) Targeting CRL4 suppresses chemoresistant ovarian cancer growth by inducing mitophagy. *Signal Transduct Target Ther* 7: 388

Metzen E, Berchner-Pfannschmidt U, Stengel P, Marxsen JH, Stolze I, Klinger M, Huang WQ, Wotzlaw C, Hellwig-Burgel T, Jelkmann W *et al* (2003) Intracellular localisation of human HIF-1 alpha hydroxylases: implications for oxygen sensing. *J Cell Sci* 116: 1319 – 1326

Mungai PT, Waypa GB, Jairaman A, Prakriya M, Dokic D, Ball MK, Schumacker PT (2011) Hypoxia triggers AMPK activation through reactive oxygen species-mediated activation of calcium release-activated calcium channels. *Mol Cell Biol* 31: 3531 – 3545

Murray JK, Balan C, Allgeier AM, Kasparian A, Viswanadhan V, Wilde C, Allen JR, Yoder SC, Biddlecome G, Hungate RW *et al* (2010) Dipeptidyl-quinolone derivatives inhibit hypoxia inducible factor-1alpha prolyl hydroxylases-1, -2, and -3 with altered selectivity. *J Comb Chem* 12: 676 – 686

Nakazawa MS, Keith B, Simon MC (2016) Oxygen availability and metabolic adaptations. *Nat Rev Cancer* 16: 663 – 673

Papandreou I, Cairns RA, Fontana L, Lim AL, Denko NC (2006) HIF-1 mediates adaptation to hypoxia by actively downregulating mitochondrial oxygen consumption. *Cell Metab* 3: 187 – 197

Percy MJ, Zhao Q, Flores A, Harrison C, Lappin TR, Maxwell PH, McMullin MF, Lee FS (2006) A family with erythrocytosis establishes a role for prolyl hydroxylase domain protein 2 in oxygen homeostasis. *Proc Natl Acad Sci U S A* 103: 654 – 659

Picard M, Shirihai OS (2022) Mitochondrial signal transduction. *Cell Metab* 34: 1620 – 1653

Pientka FK, Hu J, Schindler SG, Brix B, Thiel A, Johren O, Fandrey J, Berchner-Pfannschmidt U, Depping R (2012) Oxygen sensing by the prolyl-4-hydroxylase PHD2 within the nuclear compartment and the influence of compartmentalisation on HIF-1 signalling. *J Cell Sci* 125: 5168 – 5176

Rane S, He M, Sayed D, Vashistha H, Malhotra A, Sadoshima J, Vatner DE, Vatner SF, Abdellatif M (2009) Downregulation of miR-199a derepresses hypoxia-inducible factor-1alpha and Sirtuin 1 and recapitulates hypoxia preconditioning in cardiac myocytes. *Circ Res* 104: 879 – 886

Schofield CJ, Ratcliffe PJ (2004) Oxygen sensing by HIF hydroxylases. *Nat Rev Mol Cell Biol* 5: 343 – 354

Semenza GL (2012) Hypoxia-inducible factors: mediators of cancer progression and targets for cancer therapy. *Trends Pharmacol Sci* 33: 207 – 214

Siegel RL, Miller KD, Fuchs HE, Jemal A (2022) Cancer statistics, 2022. *CA Cancer J Clin* 72: 7 – 33

Takeda K, Ho VC, Takeda H, Duan LJ, Nagy A, Fong GH (2006) Placental but not heart defects are associated with elevated hypoxia-inducible factor alpha levels in mice lacking prolyl hydroxylase domain protein 2. *Mol Cell Biol* 26: 8336 – 8346

Tan JX, Finkel T (2020) Mitochondria as intracellular signaling platforms in health and disease. *J Cell Biol* 219: e202002179

Trefts E, Shaw RJ (2021) AMPK: restoring metabolic homeostasis over space and time. *Mol Cell* 81: 3677 – 3690

Valcarcel-Jimenez L, Gaude E, Torrano V, Frezza C, Carracedo A (2017) Mitochondrial metabolism: Yin and Yang for tumor progression. *Trends Endocrinol Metab* 28: 748 – 757

Wang Z, Liu P, Chen Q, Deng S, Liu X, Situ H, Zhong S, Hann S, Lin Y (2016) Targeting AMPK signaling pathway to overcome drug resistance for cancer therapy. *Curr Drug Targets* 17: 853 – 864

Waypa GB, Marks JD, Mack MM, Boriboun C, Mungai PT, Schumacker PT (2002) Mitochondrial reactive oxygen species trigger calcium increases during hypoxia in pulmonary arterial myocytes. *Circ Res* 91: 719 – 726

Wotzlaw C, Gneuss S, Konietzny R, Fandrey J (2010) Nanoscopy of the cellular response to hypoxia by means of fluorescence resonance energy transfer (FRET) and new FRET software. *PMC Biophys* 3: 5

Yan C, Gong L, Chen L, Xu M, Abou-Hamdan H, Tang M, Desaubry L, Song Z (2020) PHB2 (prohibitin 2) promotes PINK1-PRKN/Parkin-dependent mitophagy by the PARL-PGAM5-PINK1 axis. *Autophagy* 16: 419 – 434

Yang H, Kaelin WG Jr (2001) Molecular pathogenesis of the von Hippel-Lindau hereditary cancer syndrome: implications for oxygen sensing. *Cell Growth Differ* 12: 447 – 455

Ye Y, Hu Q, Chen H, Liang K, Yuan Y, Xiang Y, Ruan H, Zhang Z, Song A, Zhang H *et al* (2019) Characterization of hypoxia-associated molecular features to aid hypoxia-targeted therapy. *Nat Metab* 1: 431 – 444

Zhang Q, Gu J, Li L, Liu J, Luo B, Cheung HW, Boehm JS, Ni M, Geisen C, Root DE *et al* (2009) Control of cyclin D1 and breast tumorigenesis by the EglN2 prolyl hydroxylase. *Cancer Cell* 16: 413 – 424

Zhang J, Wang C, Chen X, Takada M, Fan C, Zheng X, Wen H, Liu Y, Wang C, Pestell RG *et al* (2015) EglN2 associates with the NRF1-PGC1alpha complex and controls mitochondrial function in breast cancer. *EMBO J* 34: 2953 – 2970

Zhang J, Wu T, Simon J, Takada M, Saito R, Fan C, Liu XD, Jonasch E, Xie L, Chen X *et al* (2018) VHL substrate transcription factor ZHX2 as an oncogenic driver in clear cell renal cell carcinoma. *Science* 361: 290 – 295

Zhou G, Myers R, Li Y, Chen Y, Shen X, Fenyk-Melody J, Wu M, Ventre J, Doebber T, Fujii N *et al* (2001) Role of AMP-activated protein kinase in mechanism of metformin action. *J Clin Invest* 108: 1167 – 1174

Zurlo G, Liu X, Takada M, Fan C, Simon JM, Ptacek TS, Rodriguez J, von Kriegsheim A, Liu J, Locasale JW *et al* (2019) Prolyl hydroxylase substrate adenylosuccinate lyase is an oncogenic driver in triple negative breast cancer. *Nat Commun* 10: 5177